ACS Chemical Neuroscience

Article

Fascaplysin Derivatives Are Potent Multi-target Agents Against Alzheimer's Disease: in vitro and in vivo Evidence

Hanbo Pan, Hongda Qiu, Ke Zhang, Panpan Zhang, Weida Liang, Mengxiang Yang, Chenye Mou, Miaoman Lin, Ming He, Xiao Xiao, Difan Zhang, Haixing Wang, Fufeng Liu, Yongmei Li, Haixiao Jin, Xiaojun Yan, Hongze Liang, and Wei Cui

ACS Chem. Neurosci., **Just Accepted Manuscript** • Publication Date (Web): 22 Oct 2019

Fascaplysin Derivatives Are Potent Multi-target Agents Against Alzheimer's Disease: *in vitro* and *in vivo* Evidence

Hanbo Pan [1], Hongda Qiu [2], Ke Zhang [1], Panpan Zhang [1], Weida Liang [1], Mengxiang Yang [1], Chenye Mou [1], Miaoman Lin [2], Ming He [2], Xiao Xiao [1], Difan Zhang [1], Haixing Wang [3], Fufeng Liu [4], Yongmei Li [2], Haixiao Jin [5], Xiaojun Yan [5], Hongze Liang [2,*] and Wei Cui [1,4,*]

[1] Ningbo Key Laboratory of Behavior Neuroscience, Zhejiang Province Key Laboratory of Pathophysiology, School of Medicine, Ningbo University, Ningbo, 315211, China.

[2] School of Materials Science and Chemical Engineering, Ningbo University, Ningbo, 315211, China.

[3] Zhejiang Province Key Laboratory of Anesthesiology, Department of Anesthesiology, The Second Affiliated Hospital and Yuying Children's Hospital of Wenzhou Medical University, Wenzhou, 325000, China.

[4] State Key Laboratory of Food Nutrition and Safety, College of Biotechnology, Tianjin University of Science & Technology, Tianjin, 300457, China.

[5] Li Dak Sum Yip Yio Chin Kenneth Li Marine Biopharmaceutical Research Center, College of Food and Pharmaceutical Sciences, Ningbo University, Ningbo, 315800, China.

[*] Corresponding author: Prof. Hongze Liang, School of Materials Science and Chemical Engineering, Ningbo University, Zhejiang, China. Email: lianghongze@nbu.edu.cn.

and Dr. Wei Cui, Department of Physiology, School of Medicine, Ningbo University, Zhejiang, China. Email: cuiwei@nbu.edu.cn.

Abstract

Alzheimer's disease (AD) is characterized by the progressive neurodegeneration and the impaired cognitive functions. Fascaplysin is a β-carboline alkaloid isolated from marine sponge *Fascaplysinopsis Bergquist* sp. in 1988. Previous studies have shown that fascaplysin might act on acetylcholinesterase and β-amyloid (Aβ) to produce anti-AD properties. In this study, a series of fascaplysin derivatives were synthesized. The cholinesterase inhibition activities, the neuronal protective effects, and the toxicities of these compounds were evaluated *in vitro*. **2a** and **2b**, the two most powerful compounds *in vitro*, were further selected to evaluate their cognitive-enhancing effects in animals. Both **2a** and **2b** could ameliorate cognitive dysfunction induced by scopolamine or Aβ oligomers, respectively, without affecting locomotor functions in mice. We also found that **2a** and **2b** could prevent cholinergic dysfunctions, decrease pro-inflammatory cytokines expression, and inhibit Aβ-induced tau hyper-phosphorylation *in vivo*. Most importantly, pharmacodynamics studies suggested that **2b** could penetrate the blood-brain barrier, and retain in the central nervous system. All these results suggested that fascaplysin derivatives are potent multi-target agents against AD, and might be clinical useful for AD treatment.

Keywords: Alzheimer's disease; fascaplysin; acetylcholinesterase; β-amyloid; neuroinflammation; oxidative stress.

Abbreviations

AD, Alzheimer's disease; AChE, acetylcholinesterase; ANOVA, analysis of variation; ATCI, acetylthiocholine iodide; Aβ, amyloid-β; BBB, Blood Brain Barrier; BuChE, butylcholinesterase; CAS, catalytic site residue; CNS, central nervous system; ChAT, choline acetyltransferase; ELISA, enzyme-linked immunosorbent assay; FDA, fluorescein diacetate; IL-1β, interleukin-1β; IL-6, interleukin-6; IL-10, interleukin-10; IL-17, interleukin-17; *i.p.,* intraperitoneal; MWM, Morris water maze; NF-κB, nuclear factor-κB; NOR, novel object recognition; PAS, peripheral anionic site; PI, propidium iodide; ROS, reactive oxygen species; SI, the selectivity index; TNF-α, tumor necrosis factor-α.

Introduction

Alzheimer's disease (AD) is the most common dementia among elderly characterized by cognitive impairments such as learning and memory dysfunction[1]. Unfortunately, there is no drug could effectively reverse the injury and death caused by AD, the severe threat to global public health which is believed to be a complex disease with various pathological factors[2]. Acetylcholinesterase (AChE) plays a core role in cholinergic transmission through the hydrolysis of the neurotransmitter acetylcholine[3]. It is widely accepted that the dysfunction of the cholinergic system, including the enhancement of AChE activity and the decline of choline acetyltransferase (ChAT) level in brains, is the direct cause leading to cognitive impairments in AD patients[4]. Besides, neuroinflammation is widely found in the brain of AD patients, causing the death of neurons[5]. Many pro-inflammatory cytokines such as interleukin (IL)-1β, IL-6, IL-17 and tumor necrosis factor-α (TNF-α), could lead to neuroinflammation, and accelerate neuronal injury[6]. Moreover, the anti-inflammatory cytokines, particularly IL-10, are down-regulated in AD brains[7]. Furthermore, β-amyloid (Aβ) is considered to be one of the major neurotoxins leading to AD[8]. Aβ can automatically form into various aggregates, among which Aβ oligomers are the most toxic specie to induce neurotoxicity[9]. Aβ could induce the hyper-phosphorylation of tau, a microtubule-associated protein, and lead to the instability of cytoskeleton and neuronal injuries[10-11]. Hyper-phosphorylated tau could form into neurofibrillary tangles, one of the major hallmarks of AD. Furthermore, free radicals in AD brain could cause oxidative stress and result in neuronal degeneration[12-13].

The multiple pathological mechanisms of AD indicated that single-target drugs might have limited efficacy, while the multi-target drugs could have superiorities when compared with single-target agents[14]. Multi-target drugs could act on various targets simultaneously, thus possess good efficacy. Besides, multi-target drugs could overcome the deficits of the combining use of drugs with good bioavailability and pharmacokinetic characteristics. Furthermore, multi-target drugs could enhance the compliance of patients[15]. Therefore, the development of multi-target agents is a promising strategy for the searching of effective anti-AD drugs[16].

Fascaplysin is a fused benzoyl-linked β-carboline alkaloid firstly derived from marine sponge *Fascaplysinopsis Bergquist* sp. near Fiji Island in 1988[17]. Fascaplysin could inhibit cyclin-dependent kinases 4 to prevent ovarian cancer cell proliferation and metastasis, and increase suicidal erythrocyte death[18-20]. Moreover, fascaplysin was reported to inhibit AChE with IC_{50} at around 1.5 μM, suggesting this compound might be used to treat AD[21]. Recently, it was reported that fascaplysin could preferably prevent Aβ aggregation, and protect against Aβ oligomers-induced neuronal death[22]. However, it is largely unknown whether fascaplysin derivatives can act on other AD-related targets. Moreover, it is not certain whether fascaplysin derivatives could produce *in vivo* cognitive-enhancing effects, and whether fascaplysin derivatives could penetrate the blood-brain barrier (BBB) to exert their functions.

H_2O_2 is a typical non-radical oxygen derivative which could penetrate easily through cell membranes and lead to neurotoxicity[23-24]. H_2O_2-induced neurotoxicity is a classical research model for screening neuroprotective agents[25]. Scopolamine can compete with acetylcholine for postsynaptic membrane receptors, resulting in acute cholinergic dysfunctions[26]. Intrahippocampal injection of Aβ oligomers could induce neurotoxicity, and produce cognitive impairments and neuroinflammation in mice[27]. Therefore, scopolamine and Aβ oligomers-induced dementia animal models have been widely used to screen potential cognitive-enhancing agents.

In this study, we have synthesized a series of β-carboline and fascaplysin derivatives, and further evaluated their cholinesterase inhibition and neuroprotective activity *in vitro*. The toxicities of these compounds were also tested in SH-SY5Y cells. The cognitive-enhancing effects of two most potent compounds, **2a** and **2b**, were further studied in scopolamine- and Aβ oligomers-treated mice, respectively. The preliminary toxicological and pharmacodynamics properties of representative fascaplysin derivatives were also tested *in vivo*.

Results and Discussions

Synthesis of β-carboline and fascaplysin derivatives

Synthesis schemes of compounds **1a-1e**, **1h-1i** and **2a-2e**, **2h-2i** were illustrated in Fig. 1A, while synthesis of **1f-1g**, **1j-1k** and **2f-2g** was described in Fig. 1B. β-carbolines and methyl-substituted derivatives **1** and corresponding fascaplysins **2** were prepared according to the published procedure[22,28-30]. Carboxylic β-carboline **1e** underwent thermo-induced intramolecular nucleophilic substitution to yield **2e**. Amide-modified β-carbolines were synthesized by condensation between acyl chloride prepared in situ and amine. Following cyclization reaction afforded amide-modified fascaplysin. Reduction of amido carboline **1g** by $LiAlH_4$ gave hydroxy derivative **1k**. The synthesized chemicals were characterized by FTIR, HRMS, ^{1}H NMR and ^{13}C NMR spectroscopy and HPLC (Supporting information: Figs. S1-S40, Tables. S1-S21).

To evaluate the anti-AD efficacy of the synthesized fascaplysin derivatives, we screened the chemical library by measuring cholinesterase inhibition and anti-oxidative stress abilities *in vitro*. The promising chemicals were chose for further *in vivo* tests to evaluate their efficacies of ameliorating cognitive impairments induced by scopolamine and Aβ oligomers, respectively. Subsequently, their abilities of preventing cholinergic system dysfunction, reducing neuroinflammation, and inhibiting the hyper-phosphorylation of tau were tested. Additionally, the preliminary toxicological and pharmacodynamics properties of representative compounds were also investigated.

Fascaplysin Derivatives Effectively Inhibit Cholinesterase *in vitro*

β-carboline alkaloids, also known as harmine alkaloids, were first discovered in *Pergamum harmala*, and have lots of biological activities, including anti-tumor, anti-malaria and anti-inflammation activities[31]. Recently, many studies have reveled that β-carboline alkaloids could effectively inhibit cholinesterase and reduce oxidative stress, suggesting that they might possess neuroprotective abilities and are promising agents for the development of neuroprotective drugs[32]. Thus, we firstly screened compounds library using AChE and butylcholinesterase (BuChE) activity assay *in vitro*. Moreover, the selectivity index (SI) value was calculated by using the equation of IC_{50} (BuChE) / IC_{50} (AChE). AChE inhibitors were clinically used in the treatment of AD. BuChE is a nonspecific cholinesterase that hydrolyses many different choline-based esters. Our results found that **1a**-**1i** and **2f** could not inhibit AChE or BuChE activities even as high as 1 mM (Table 1). **2a**-**2e** could potently inhibit AChE (**2a**, IC_{50} =1.21 ± 0.04 μM; **2b**, IC_{50} = 0.95 ± 0.10 μM; **2c**, IC_{50} = 2.92 ± 0.09 μM; **2d**, IC_{50} = 2.32 ± 0.58 μM; and **2e**, IC_{50} = 9.55 ± 1.23 μM) and BuChE (**2a**, IC_{50} = 8.63 ± 1.01 μM; **2b**, IC_{50} = 2.79 ± 0.76 μM; **2c**, IC_{50} = 11.11 ± 1.93 μM; **2d**, IC_{50} = 6.19 ± 0.87 μM; and **2e**, IC_{50} = 15.98 ± 1.19 μM) with IC_{50} values at micromolar ranges (Table 1). **2g** could inhibit BuChE activity with the IC_{50} value of 2.90 ± 0.21 μM. However, this compound could not inhibit AChE activity even as high as 1 mM (Table 1).

The inhibition activities of **2a**-**2e** against AChE were stronger than those against BuChE (**2a**, SI = 7.13; **2b**, SI = 2.94; **2c**, SI = 3.81; **2d**, SI = 2.67 and **2e**, SI = 1.67), which might be due to the structural differences between two enzymes. Interestingly, **2b** was more potent to inhibit cholinesterase activity than **2a**, its original compound, suggesting that the modification of fascaplysin could improve its cholinesterase inhibition effects.

We further explored whether the anion of particular fascaplysin derivative has effects on its cholinesterase inhibition activity. **2h** and **2i** have same structures as those of **2a** and **2b**, with only the different anions. **2h** and **2i** could inhibit cholinesterase with similar IC_{50} values compared with **2a** and **2b**, respectively (Table 1). These results indicated that the anion might not significantly influence cholinesterase inhibition activities of the synthesized compounds. To further demonstrate how **2b** acts on AChE, two concentrations (0.20 and 0.80 μM) of **2b** were used. Lineweaver–Burk plot showed that **2b** inhibited AChE with a K_i value of 2.60 μM (Figs. 2A-2B).

In order to explain the different AChE inhibition efficacies of fascaplysin derivatives, molecular docking analysis was performed. Fascaplysin was reported to bind only to the peripheral anionic site (PAS) of AChE[21]. Our docking analysis suggested that **2b** might bind not only to the PAS residues such as Tyr341, Trp286, Phe338 and Tyr337 through π-π interaction, but also to Trp86 in the catalytic site residue (CAS) through C-H and π interaction, leading to the enhanced AChE inhibition ability (Fig. 2C). Meanwhile, **2c** might have similar binding mode with AChE comparing with **2b**, except for the substituted 8-methyl group. Instead of forming C-H and π interaction with

the benzene ring of Trp86, the 8-methyl group of **2c** formed hydrophobic interaction with the methylene group in the side chain of Trp86, leading to a certain reduction of AChE inhibition of **2c** (Fig. 2D). **2d** and **2e** could also bind to PAS and CAS of AChE. However, the electron-withdrawing substituted bromine in **2d**, and the negative charged carboxyl in **2e** have different levels of electron repulsion with aromatic ring of Trp86 in CAS, and lead to the declined AChE inhibition abilities of **2d** and **2e** when compared with **2b** (Figs. 2E-2F). Similarly, the electron repulsion between negative charged carbamoyl of **2f** and aromatic ring of Trp86 in CAS might greatly decline AChE inhibition effects of **2f**.

Furthermore, fascaplysin derivatives are planar conjugated pentacyclic molecules, and could easily enter into the gorge of AChE. However, β-carboline derivatives are more flexible than fascaplysin derivatives, and the benzene ring of β-carboline derivatives could rotate alone its axis. Therefore, we conjectured that **1a**-**1k** could not smoothly enter into the gorge of AChE, which lead to the decreased AChE inhibition. Similarly, the big substituents in **2g** might result in the unsuccessful entry into the gorge of AChE.

AChE could catalyze the decomposition of acetylcholine, preventing the conduction of nerve impulse among cholinergic neurons. Thus, the increasing activity of AChE could directly lead to the cognitive impairments in AD patients. AChE inhibitors, such as donepezil, rivastigmine and galanthamine, are clinical used for the treatment of AD. There are lots of studies in the development of AChE inhibitors based on β-carboline structure[33-34]. It was reported a harmine derivative inhibited AChE with IC_{50} value of 1.90 μM[33]. Moreover, there are 23 kinds of bivalent β-carboline derivatives with AChE inhibition activities among which the most powerful compound inhibited AChE with IC_{50} value of 9.60 μM[34]. Our results showed that **2b**, the most potent fascaplysin derivative, could inhibit AChE with the IC_{50} value within 1 μM, suggesting **2b** might be one of the most powerful AChE inhibitors based on β-carboline structure.

Fascaplysin Derivatives Extenuate H_2O_2-indcued Neurotoxicity in SH-SY5Y Cells

Referring to the results of AChE activity assay, **2a, 2b, 2c, 2d and 2e**, the five potent AChE inhibitors, was selected for further neuroprotective evaluation. The neuroprotective ability of fascaplysin derivatives was evaluated by using H_2O_2-induced neuronal death model in SH-SY5Y cells. Fucoxanthin is an effective antioxidant which could reduce oxidative stress and protect SH-SY5Y cells against H_2O_2-induced apoptosis *in vitro*[35]. Therefore, fucoxanthin was chose as a positive control in the study. Tacrine and curcumin were also tested in the same model. SH-SY5Y cells were pre-treated by various concentrations of tested compounds for 1 h, followed by the treatment with 0.3 mM H_2O_2 for 24 h. The results showed that **2a**, **2b** and **2d** significantly protected SH-SY5Y cells against H_2O_2-induced neuronal death at the concentration of 0.3-3.0 nM, while tacrine, curcumin and fucoxanthin showed lower neuroprotective efficacy comparing with the tested

compounds (one-way ANOVA, Tukey's test, $p < 0.01$, Fig. 2G). To further characterize the neuroprotective effects of the representative compounds, we used fluorescein diacetate/propidium iodide (FDA/PI) double staining assay. Our results showed that **2b**, the most potent anti-oxidant among fascaplysin derivatives, could substantially increase cells viability in H_2O_2-induced SH-SY5Y cells at 3 nM (one-way ANOVA, Tukey's test, $p < 0.01$, Figs. 2H-2I,).

Reactive oxygen species (ROS), such as H_2O_2, O^{2-} and ·OH, could lead to oxidative stress and induce death of neurons, and play an important role in the pathogenesis of AD[36]. Therefore, reducing ROS level is an effective way to treat AD. Our study showed that **2a**, **2b** and **2d** could decline H_2O_2-induced neurotoxicity with the concentration of nanomolar range, indicating that they might possess anti-AD neuroprotective efficacy. However, neither tacrine, a potent AChE inhibitor, nor curcumin, an Aβ aggregation inhibitor, could produce significant neuroprotection against H_2O_2-induced apoptosis at the similar concentration[22,37]. These studies suggested that **2a**, **2b** and **2d** might act on the targets apart from AChE and Aβ to protect neurons. Interestingly, the effective neuroprotective concentrations of **2b** obeyed the bell-shaped dose response curve peaking at 0.3 nM. The bell-shaped dose response curve could be widely found in pharmacological research with the following possible reasons. 1) High concentration of drugs might lead to desensitization of the particular receptors, and further result in the decline of the biological effects[38-39]. **2b** is a hydrophilic molecule, and likely binds to the receptors on cell membrane. We anticipated that high concentration of **2b** might desensitize the receptors that related to the neuroprotection, and lead to the decrease of neuroprotection. 2) Drugs might simultaneously act on various targets, and total effects could be the composition of the individual effects of drugs on these targets[40]. It was reported that harmine could reduce oxidative stress via activating catalase, glutathione peroxidase and superoxide dismutase in mice[31]. Therefore, we conjectured that **2b** might act on enzymes involving in the production and cleavage of ROS. Low concentrations of **2b** might mainly activate the anti-oxidant enzymes to produce its neuroprotective effects. However, high concentrations of **2b** might lead to the activation of the oxidase, such as L-amino-acid oxidase and D-amino-acid oxidase to produce ROS, further resulting in the reduction of the neuroprotective efficacy of **2b**. However, the detailed neuroprotective mechanism of **2b** has not been fully elucidated yet, and our lab is performing experiments to investigate this issue.

2a and 2b Effectively Attenuate Scopolamine-induced Cognitive Impairments, Cholinergic Dysfunctions and Neuroinflammation *in vivo*

Based on the activities of AChE inhibition and neuroprotection, we have selected **2a** and **2b** for the further *in vivo* tests. Cholinergic system dysfunction is regarded as the major reason that induce learning and memory impairments in AD patients[41]. Meanwhile, neuroinflammation could lead to neuronal degeneration, and play an important role in AD pathogenesis[42]. Scopolamine can induce cholinergic system dysfunction and neuroinflammation in mice[43]. Therefore, acute administration

of scopolamine was used to establish an AD animal model. Donepezil is widely used as a positive control in the development of novel AChE inhibitors[44]. Intraperitoneal (*i.p.*) injection of donepezil at the dose of 3-5 mg/kg was reported to prevent cholinergic dysfunctions and reduce neuroinflammation in the hippocampus of mice[5,45]. Therefore, 4 mg/kg donepezil was *i.p.* injected daily 45 min before the animal behavior tests as a positive control. However, the pharmacokinetics characters of **2b**, especially the efficiency to permeate BBB, were not clear. Moreover, it is unknown whether **2b** could produce peripheral side effects and toxicity in animals after *i.p.* injection. Intrahippocampal injection is a prevalent method used in neuroscience study[46-48]. Drugs could directly act on the targets in the hippocampus, and are not likely to produce peripheral side effects after intrahippocampal injections. Therefore, in our study, **2a** and **2b** was intrahippocampal injected. We have previously found that neither intrahippocampal nor *i.p.* injection of vehicle could alter cognition of mice[1,27]. Therefore, in the control and scopolamine groups, we used a pool of mice with either intrahippocampal injection or *i.p.* injection of vehicle.

The open field tests were used to evaluate whether **2a** and **2b** could affect locomotor activity of mice. None of the treatments altered numbers of line crossing [one-way ANOVA, $F(6, 49) = 0.18$, $p > 0.05$, Fig. 3A] and rearing [one-way ANOVA, $F(6, 49) = 0.408$, $p > 0.05$, Fig. 3B], suggesting that **2a** and **2b** could not affect locomotor ability of mice. These results also indicated that **2a** and **2b** could not produce strong toxicity in mice at these concentrations.

The novel object recognition (NOR) tests were used to evaluate whether **2a** and **2b** could ameliorate recognition impairments induced by scopolamine in mice. In the training session, all groups possessed similar recognition index for two identical objects [one-way ANOVA, $F(6, 49) = 0.266$, $p > 0.05$, Fig. 3C]. However, the recognition index was significantly different among the groups in the exploring session [one-way ANOVA, $F(6, 49) = 9.43$, $p < 0.01$, Fig. 3D]. The recognition index of the control group was significantly higher than that of the scopolamine group (Tukey's test, $p < 0.01$, Fig. 3D). Furthermore, donepezil, **2a** and **2b** treatment significantly increased recognition index when compared with scopolamine group (Tukey's test, $p < 0.05$, Fig. 3D). These results suggested that **2a** and **2b** were capable of preventing scopolamine-induced cognitive dysfunction. Moreover, **2b** was more potent than **2a** to improve cognitive functions in mice. We also used Morris water maze (MWM) tests to evaluate whether **2a** and **2b** could ameliorate scopolamine-induced spatial cognitive dysfunction. At the 3^{rd}-5^{th} day of training session, scopolamine significantly increased escape latency when compared with the control group [one-way ANOVA, Tukey's test, $F(6, 77) = 37.40$, $p < 0.01$, Fig. 3E]. At the 4^{th}-5^{th} day, donepezil, **2a** and **2b** treatment significantly decreased escape latency when compared with scopolamine group, indicating that representative fascaplysin derivatives could inhibit scopolamine-induced spatial learning impairments (Tukey's test, $p < 0.05$, Fig. 3E). In the probe trial, the duration in the target quadrant [one-way ANOVA, Tukey's test, $F(6, 49) = 16.03$, $p < 0.01$, Fig. 3F] and the number of platform area crossing [one-

way ANOVA, Tukey's test, F (6, 49) = 13.53, $p < 0.01$, Fig. 3G] were significantly decreased in scopolamine group when compared with the control group. Donepezil and **2b** treated mice spent a significantly longer time in the target quadrant than that of mice treated by scopolamine (Tukey's test, $p < 0.05$, Fig. 3F). In addition, donepezil, **2a** and **2b** treatment significantly increased the number of platform area crossing when compared with scopolamine-treated mice (Tukey's test, $p < 0.05$, Fig. 3G), demonstrating that **2a** and **2b** could prevent scopolamine-induced spatial memory impairments.

The ability of **2a** and **2b** to inhibit cholinergic dysfunctions and neuroinflammation were also evaluated in scopolamine-treated mice. AChE activities in the hippocampal region of mice were analyzed *in vivo*. The AChE activity in the hippocampus was significantly higher in scopolamine-treated mice when compared with the control group [one-way ANOVA, Tukey's test, F (6, 49) = 12.32, $p < 0.01$, Fig. 4A]. Donepezil, **2a** and **2b** treatment significantly decreased AChE activity when compared with the scopolamine group, indicating that both fascaplysin derivatives could inhibit scopolamine-induced increase of AChE activity (Tukey's test, $p < 0.05$, Fig. 4A). We used Western blotting assay to determine the level of ChAT. ChAT level was markedly reduced in scopolamine-treated mice when compared with the control group (one-way ANOVA, Tukey's test, $p < 0.05$, Figs. 4B-4E). **2a** (one-way ANOVA, Tukey's test, $p < 0.01$, Figs. 4B-4C) and **2b** (one-way ANOVA, Tukey's test, $p < 0.01$, Figs. 4D-4E) significantly increased ChAT level when compared with the scopolamine-treated mice, suggesting that both fascaplysin derivatives could prevent scopolamine-induced decrease of ChAT levels. These results suggested that fascaplysin derivatives could inhibit cholinergic dysfunctions induced by scopolamine in mice.

Moreover, IL-1β, IL-6, IL-10 and TNF-α levels in the hippocampus were determined by enzyme-linked immunosorbent assay (ELISA). The results showed that scopolamine significantly up-regulated IL-1β [one-way ANOVA, Tukey's test, F (6, 49) = 20.21, $p < 0.01$, Fig. 4F], TNF-α [one-way ANOVA, Tukey's test, F (6, 49) = 79.79, $p < 0.01$, Fig. 4G] and IL-6 [one-way ANOVA, Tukey's test, F (6, 49) = 30.41, $p < 0.01$, Fig. 4H] levels while down-regulated IL-10 level [one-way ANOVA, Tukey's test, F (6, 49) = 37.01, $p < 0.01$, Fig. 4I] when compared with control group. However, donepezil, **2a** and **2b** could decrease IL-1β (Tukey's test, $p < 0.01$, Fig. 4F) and TNF-α levels (Tukey's test, $p < 0.05$, Fig. 4G), and increase IL-10 level (Tukey's test, $p < 0.01$, Fig. 4I) when compared with scopolamine-treated group. Besides, IL-6 level in mice treated with **2a** and **2b** were lower than that in scopolamine-treated mice (Tukey's test, $p < 0.05$, Fig. 4H). Donepezil, **2a** and **2b** were also raised IL-10 level when compared with scopolamine-treated group (Tukey's test, $p < 0.01$, Fig. 4I). Meanwhile, IL-17 level was analyzed by Western blotting assay. IL-17 level in scopolamine-treated mice was markedly higher than that in control group (one-way ANOVA, Tukey's test, Figs. 4J-4M). And donepezil, **2a** (one-way ANOVA, Tukey's test, $p < 0.01$, Figs. 4J-4K) and **2b** (one-way ANOVA, $p < 0.01$, Figs. 4L-4M) could significantly reduce IL-17 level when

compared with scopolamine-treated mice. All these results suggested that **2a** and **2b** could inhibit neuroinflammation in mice. Scopolamine-induced cognitive impairments model is widely used as an efficient screening tool for the cognitive improving drugs[32,49-50]. In our study, **2a** and **2b** could prevent scopolamine-induced cognitive impairments via inhibiting cholinergic dysfunctions and neuroinflammation, suggesting that **2a** and **2b** might be used as anti-AD agents.

It was showed that neuroinflammation, especially those associated with the activation of microglia and release of pro-inflammatory cytokines, could contribute to neuronal degeneration in AD[18]. Activated microglia could divide into cytotoxic M1 subtype and pro-repair M2 subtype. The M1 phenotype is believed to produce pro-inflammatory cytokines, such as IL-1β, and induce neuronal injury, while the M2 phenotype could increase the clearance of neurotoxicity and enhance the remodeling of brain tissues[51]. Nuclear factor-κB (NF-κB) signaling pathway plays a core part in the activation of M1 subtype microglia. Recently, lots of studies showed β-carbolines could inhibit NF-κB pathway[52]. Thus, we conjectured that **2a** and **2b** might reduce neuroinflammation, and improve cognitive functions via inhibiting NF-κB pathway, and further preventing the activation of M1 phenotype microglia. However, the clarifying detailed mechanism requires more investigation.

2a and 2b Ameliorate Aβ Oligomers-induced Cognitive Dysfunction and Tau Hyper-phosphorylation *in vivo*

Recently, fascaplysin was reported to inhibit Aβ aggregation and produce neuroprotection *in vitro*[19]. However, whether fascaplysin derivatives could reduce neurotoxicity of Aβ *in vivo* remain unclear. Thus, we further tested whether **2a** and **2b** could prevent Aβ oligomers-induced cognitive impairments and tau hyper-phosphorylation *in vivo*.

The cognitive ability of mice were evaluated by Y maze, NOR and MWM tests. In Y maze tests, the spontaneous alteration of mice in Aβ oligomers group was significantly reduced compared with the control group, indicating that Aβ oligomers could reduce recognition in mice [one-way ANOVA, Tukey's test, $F(5, 35) = 4.831$, $p < 0.01$, Fig. 5A]. Moreover, the spontaneous alteration of mice in **2a** and **2b** groups were significantly increased compared with Aβ oligomers groups, suggesting that both of fascaplysin derivatives could prevent Aβ oligomers-induced recognition impairments (Tukey's test, $p < 0.01$, Fig. 5A). Similar results were found in the Aβ oligomers-induced cognitive impairments model, **2a** and **2b** could prevent Aβ oligomers-induced recognition and spatial cognitive impairments (one-way ANOVA, Tukey's test, Figs. 5B-5E).

We also used Western blotting assay to determine the levels of tau and hyper-phosphorylated tau in hippocampus of mice. Tau level was similar among various groups (one-way ANOVA, Tukey's test, $p > 0.05$, Figs. 5G and 5I). However, the level of hyper-phosphorylated tau in Aβ oligomers-treated group was significantly higher when compared with control group (Tukey's test, $p < 0.05$,

Figs. 5G-5J). Meanwhile, **2a** (one-way ANOVA, $p < 0.01$, Figs. 5G-5H) and **2b** (one-way ANOVA, Tukey's test, $p < 0.01$, Figs. 5I-5J) significantly decreased Aβ oligomers-induced increase of hyper-phosphorylated tau level in mice.

Aβ oligomers could lead to neuronal death and recognition dysfunction, and is believed to be the major neurotoxic aggregates for AD[53]. Aβ oligomers induced-hyper-phosphorylation of tau could disrupt the organization of microtubule, and lead to neurotoxicity. It was believed that the prevention of tau hyper-phosphorylation could effectively protect neurons and ameliorate dementia[54]. Our results indicated that **2a** and **2b** could prevent Aβ oligomers-induced learning and memory impairments through inhibiting tau hyper-phosphorylation, suggesting they might delay the pathological process of AD, and are promising drug candidates for the treatment of AD.

***In vitro* and *in vivo* Toxicity Evaluation of Fascaplysin Derivatives**

Fascaplysin was widely used for the development of anti-cancer drugs, and could induce cells apoptosis. Therefore, we tested whether fascaplysin derivatives could produce neurotoxicity both *in vitro* and *in vivo*. The *in vitro* toxicity of **2a**-**2e** was determined by MTT assay in SH-SY5Y cells. The IC_{50} values of **2a** and **2b** to inhibit cell viability were 0.09 ± 0.03 μM and 0.18 ± 0.02 μM, respectively (Table 2). At the same condition, **2c**-**2e** showed micromolar range *in vitro* neurotoxicity (**2c**, IC_{50} = 1.60 ± 0.21 μM; **2d**, IC_{50} = 5.30 ± 0.78 μM; **2e**, IC_{50} = 75.80 ± 1.06 μM, Table 2).

The acute toxicity of fascaplysin in mice (LD_{50} = 30 mg/kg) was reported in a previous study[55]. Therefore, we also evaluated the acute toxicity of **2b** in mice. Mice were treated with various concentrations of **2b** (20 -120 mg/kg) by *i.p.* injection and the survival rate was calculated after 3 days of administration. We found the LD_{50} value of **2b** was about 50 mg/kg, suggesting **2b** might possess lower toxicity when compared with fascaplysin. These results indicated that the modification of fascaplysin not only enhanced its anti-AD activity, but also reduced its toxicity.

Interestingly, our *in vitro* results showed the IC_{50} value of **2b** to inhibit AChE was about 5 times more than its IC_{50} value to inhibit SH-SY5Y cells viability, suggesting that **2b** might produce neurotoxicity in effective AChE inhibition concentration *in vitro*. However, it may not be proper to conclude that **2b** has neurotoxicity when effectively inhibiting AChE *in vivo*. The *in vivo* effects of **2b** might be largely influenced by drug distribution and metabolism. The metabolites of chemicals might also have biological effects with different degree of efficacy. In our *in vivo* study, we found that **2b** effectively inhibited AChE in the hippocampus of mice, and prevented cognitive impairments without performing severe neurotoxicity. In addition, the acute toxicity study showed the LD_{50} value of **2b** on mice was 50 mg/kg, which was lower than the clinical used anti-AD drugs. All these results suggested that **2b** might not produce toxicity when effectively exhibiting anti-AD effects *in vivo*.

2b Could Penetrate BBB and Retain in the Central Nervous System

We further evaluated whether representative fascaplysin could penetrate BBB. **2b** was predicted to be able to penetrate into the brain by the software of ACD/Percepta. **2b** at 30 mg/kg was administrated into mice by tail vein injection. At 15 min after drug administration, the brain and the blood samples were collected and analyzed by the ultra-performance liquid chromatography-tandem mass spectrometry (UPLC-MS/MS). It was found that the concentrations of **2b** in the blood and brain were 6.3 μg/mL and 37.4 ng/mL, respectively (Supporting information: Fig. S41). These results suggested that **2b** could readily cross BBB and retain in the brain, indicating that **2b** might be developed as drugs for neurological diseases.

Conclusion

Due to the complex pathological factors of AD, one-molecule multi-target approach might provide a novel method for the development of anti-AD drugs. In this study, a series of fascaplysin derivatives were synthesized and biologically evaluated as novel multi-target drugs for the treatment of AD. The cholinesterase inhibition ability of fascaplysin derivatives was evaluated *in vitro,* and potent compounds, **2a**-**2e**, were further evaluated for their neuroprotection against H_2O_2-induced neurotoxicity. Our results indicated that **2a**, **2b** and **2d** could effectively reduce neurotoxicity at nanomolar range. Two AD mice models were used to further evaluate the anti-AD effects of **2a** and **2b** *in vivo*. The results indicated that both **2a** and **2b** could prevent cognitive impairments via inhibiting AChE activity, preventing cholinergic dysfunctions, decreasing neuroinflammation, and reducing tau hyper-phosphorylation, concurrently. **2b**, the representative fascaplysin derivatives, could also penetrate BBB, and produce *in vivo* acute toxicity lower than fascaplysin. Our study showed that fascaplysin derivatives are potent multi-target agents against AD, and **2b** might be developed as a potential agent for AD treatment.

Materials and methods

Chemistry

General Information All chemicals and solvents were purchased from commercial suppliers and used without purification, unless noted otherwise. Reactions were conducted under nitrogen atmosphere and monitored by thin layer chromatography on silica plate. Purification of products by chromatography was carried out on silica gel 200-300 mesh. Fourier transform infrared spectroscopy was measured on a Nicolet 6700 FT-IR spectrometer (Thermo Fisher, Waltham, MA, USA). NMR spectra were recorded on Bruker Avance 300, or 400 spectrometers. High resolution mass spectra were obtained on a LTQ-Orbit trap XL spectrometer (Thermo Fisher), an Agilent 6520 QTOF mass spectrometer (Agilent, Santa Clara, CA, USA) or a Bruker micrOTOF-Q II system using electrospray ionization (ESI) in positive mode. Purity analysis was conducted on a HPLC instrument (CXTH-LC-3000) using Welch Ultimate® Plus C18 column (5 μm, 4.6 mm X 250 mm),

eluting at flow rate of 1 mL/min, and monitoring at wavelength of 280 nm.

General Procedures Carbolines **1a**, **1b**, **1c**, **1d**, **1e, 1h and 1i** were prepared according to the published procedures in literature, and spectroscopic characterizations are in agreement with those reported[30]. **1f**, **1g** and **1j** were prepared by acyl chloride with respective amines. **1k** was prepared by reduction of **1g** with $LiAlH_4$. **2b** and **2h** were reported previously[22]. **2a**, **2c**, **2d**, **2e**, **2f, 2g** and **2i** were prepared according to the published procedure.

*6-bromo-9H-pyrido[3,4-b]indol-1-yl)(2-bromophenyl)methanone (**1d**)* Pale Yellow solid; m.p. 167 °C. ^{1}H NMR (400 MHz, DMSO-d6) δ 12.36 (s, 1H), 8.62 (d, J = 1.9 Hz, 1H), 8.55 - 8.42 (m, 2H), 7.84 - 7.70 (m, 3H), 7.62 - 7.49 (m, 2H), 7.52 - 7.43 (m, 1H). ^{13}C NMR (101 MHz, DMSO-d6) δ 197.23, 141.58, 141.09, 138.62, 135.93, 135.87, 132.79, 132.13, 131.69, 130.71, 129.91, 127.69, 125.05, 122.39, 120.66, 119.37, 115.58, 113.01. HRMS (ESI) (positive mode): m/z calculated for $C_{18}H_{10}Br_2N_2O$: 430.9212; $(M+H)^+$, found: 430.9210.

*1-(2-bromobenzoyl)-9H-pyrido[3,4-b]indole-6-carboxamide (**1f**)* To a solution of acid **1e** (0.20 g, 0.47 mmol, 1 equiv) and Et_3N (0.24 g, 2.3 mmol, 5equiv) in THF (3 mL) in ice-bath, thionyl chloride (3 mL) was added. The reaction was refluxed for 2 h. Excess thionyl chloride was removed under reduced pressure before ammonium chloride (0.028 g, 0.52 mmol) in THF (3 mL) was added. The reaction mixture was stirred at room temperature overnight. After removal of THF, the residue was subjected to chromatography on silica gel using EtOAc/PE as eluent. After purification, 0.124 g of **1f** was yielded (67%). Pale Yellow solid; m.p. 246 °C. FTIR (KBr, cm^{-1}): 3482, 3423, 3253, 2962, 2922, 2853, 1669, 1643, 1600, 1485, 1460, 1389, 1368, 1283, 1262, 1247, 1212, 1123, 1058, 1023, 983, 896, 841, 770, 731, 669, 635, 596, 447. ^{1}H NMR (400 MHz, DMSO-d6) δ 12.40 (s, 1H), 8.88 (d, J = 1.8 Hz, 1H), 8.46 (s, 2H), 8.15 (dd, J = 8.6, 1.8 Hz, 1H), 8.12 (s, 1H), 7.84 (d, J = 8.6 Hz, 1H), 7.72 (d, J = 7.9 Hz, 1H), 7.58 – 7.50 (m, 2H), 7.47 (td, J = 7.4, 2.4 Hz, 1H), 7.36 (s, 1H). ^{13}C NMR (101 MHz, DMSO-d6) δ 197.27, 168.88, 144.00, 141.44, 138.93, 136.23, 135.84, 132.74, 131.81, 131.73, 129.76, 129.09, 127.72, 126.95, 122.40, 120.21, 120.03, 119.24, 112.96. HRMS (ESI) (positive mode): m/z calculated for $C_{19}H_{12}BrN_3O_2$: 394.0186; $(M+H)^+$, found: 394.0185.

*1-(2-bromobenzoyl)-N-phenyl-9H-pyrido[3,4-b]indole-6-carboxamide (**1g**)* **1g** was synthesized by the same procedure as **1f** using aniline. Pale Yellow solid (70%); m.p. 218 °C. ^{1}H NMR (400 MHz, DMSO-d6) δ 12.51 (s, 1H), 10.39 (s, 1H), 9.02 (d, J = 1.1 Hz, 1H), 8.55 (dd, J = 17.0, 4.9 Hz, 2H), 8.26 (dd, J = 8.6, 1.6 Hz, 1H), 7.95 (d, J = 8.6 Hz, 1H), 7.84 (d, J = 7.7 Hz, 2H), 7.76 (d, J = 7.4 Hz, 1H), 7.61 (dd, J = 7.5, 1.8 Hz, 1H), 7.59 - 7.53 (m, 1H), 7.50 (td, J = 7.6, 1.9 Hz, 1H), 7.40 (t, J = 7.9 Hz, 2H), 7.14 (t, J = 7.4 Hz, 1H). ^{13}C NMR (101 MHz, DMSO-d6) δ 196.96, 165.92, 143.88, 141.25, 139.46, 138.72, 136.04, 135.71, 132.50, 131.56, 131.43, 129.60, 129.02, 128.80, 127.56, 127.42, 123.75, 122.36, 120.56, 120.08, 119.80, 119.06, 112.93. HRMS (ESI) (positive mode): m/z

calculated for $C_{25}H_{16}BrN_3O_2$: 470.0499; $(M+H)^+$, found: 470.0477.

*1-(2-bromobenzoyl)-N-(2-(5-methyl-1H-indol-3-yl)ethyl)-9H-pyrido[3,4-b]indole-6-carboxamide (**1j**)* **1j** was synthesized by the same procedure as **1f** using 5-methyl tryptamine. Pale Yellow solid (62%); m.p. 237 °C. ^{1}H NMR (400 MHz, DMSO-d6) δ 12.41 (s, 1H), 10.66 (s, 1H), 8.87 (s, 1H), 8.66 (t, J = 5.7 Hz, 1H), 8.48 (q, J = 4.9 Hz, 2H), 8.15 (dd, J = 8.7, 1.6 Hz, 1H), 7.86 (d, J = 8.6 Hz, 1H), 7.74 (d, J = 8.0 Hz, 1H), 7.63 – 7.43 (m, 3H), 7.39 (s, 1H), 7.23 (d, J = 8.2 Hz, 1H), 7.16 (s, 1H), 6.89 (d, J = 8.0 Hz, 1H), 3.66 – 3.57 (m, 2H), 2.99 (t, J = 7.5 Hz, 2H), 2.35 (s, 3H). ^{13}C NMR (101 MHz, DMSO-d6) δ 197.27, 166.82, 143.90, 141.63, 138.90, 136.30, 135.94, 135.09, 132.79, 131.89, 131.69, 129.91, 128.81, 128.03, 127.82, 127.70, 127.04, 123.20, 122.97, 122.04, 120.19, 120.07, 119.38, 118.46, 113.01, 111.96, 111.55, 40.98, 25.78, 21.73. HRMS (ESI) (positive mode): m/z calculated for $C_{30}H_{23}BrN_4O_2$: 551.1077; $(M+H)^+$, found: 551.1071.

*1-((2-bromophenyl)(hydroxy)methyl)-N-phenyl-9H-pyrido[3,4-b]indole-6-carboxamide (**1k**)* To a mixture of **1j** (0.20 g, 0.42 mmol) and $LiAlH_4$ (21 mg, 0.55 mmol), was added anhydrous THF at 0 °C under N_2 atmosphere. The suspension was stirred 10 min at 0 °C before refluxing for 8 h. Water was added to quench the reaction. Solvents were removed under vacuum and the residue was eluted with a solvent mixture of petroleum and ethyl acetate (V/V, 2/1) on a silica gel chromatography to give yellow solid (0.11 g, 55%). m.p. 124-125 °C. ^{1}H NMR (400 MHz, DMSO-d6) δ 11.92 (s, 1H), 10.29 (s, 1H), 8.92 (d, J = 1.7 Hz, 1H), 8.23 (d, J = 5.2 Hz, 1H), 8.18 (dd, J = 8.6, 1.8 Hz, 1H), 8.10 (d, J = 5.2 Hz, 1H), 7.91 – 7.76 (m, 3H), 7.70 (dd, J = 7.8, 1.7 Hz, 1H), 7.56 (dd, J = 8.0, 1.2 Hz, 1H), 7.46 – 7.32 (m, 3H), 7.22 (td, J = 7.7, 1.8 Hz, 1H), 7.11 (t, J = 7.4 Hz, 1H), 6.56 (s, 2H). ^{13}C NMR (101 MHz, DMSO-d6) δ 165.99, 146.18, 142.79, 142.59, 139.53, 137.80, 134.46, 132.25, 129.69, 129.10, 129.01, 128.70, 127.97, 127.50, 126.10, 123.56, 122.48, 121.91, 120.49, 120.24, 114.12, 112.14, 73.66. HRMS (ESI) (positive mode): m/z calculated for $C_{25}H_{18}BrN_3O_2$: 472.0655; $(M+H)^+$, found: 472.0642.

*13-oxo-12,13-dihydropyrido[1,2-a:3,4-b']diindol-5-ium bromide (**2a**)* Cyclization was conducted at 220 °C for 1 h. Yield: 80%; red-brown solid; m.p. > 300 °C. ^{1}H NMR (400 MHz, DMSO-d6) δ 13.51 (s, 1H), 9.60 (d, J = 6.3 Hz, 1H), 9.13 (d, J = 6.2 Hz, 1H), 8.56 (d, J = 8.0 Hz, 1H), 8.48 (d, J = 8.1 Hz, 1H), 8.06 (d, J = 7.4 Hz, 1H), 8.01 (t, J = 7.9 Hz, 1H), 7.89 (t, J = 7.8 Hz, 1H), 7.80 (d, J = 8.3 Hz, 1H), 7.74 (t, J = 7.5 Hz, 1H), 7.52 (t, J = 7.5 Hz, 1H). ^{13}C NMR (101 MHz, DMSO-d6) δ 182.77, 147.54, 147.40, 140.99, 137.51, 134.78, 131.82, 131.60, 127.18, 126.04, 124.84, 124.49, 123.52, 123.24, 120.82, 119.92, 116.09, 114.20. HRMS (ESI) (positive mode): m/z calculated for $C_{18}H_{11}N_2O$: 271.0866; $(M-Br)^+$, found: 271.0891.

*8-methyl-13-oxo-12,13-dihydropyrido[1,2-a:3,4-b']diindol-5-ium bromide (**2c**)* Cyclization was conducted at 220 °C for 1 h. Yield: 80%; dark brown solid; m.p. > 300 °C. ^{1}H NMR (400 MHz,

DMSO-d6) δ 13.48 (s, 1H), 9.52 (d, J = 6.3 Hz, 1H), 8.85 (d, J = 6.3 Hz, 1H), 8.53 (d, J = 8.0 Hz, 1H), 8.04 (d, J = 7.6 Hz, 1H), 8.01 (t, J = 7.5 Hz, 1H), 7.73 (q, J = 7.3 Hz, 2H), 7.60 (d, J = 8.2 Hz, 1H), 7.27 (d, J = 7.2 Hz, 1H), 2.89 (s, 3H). ^{13}C NMR (101 MHz, DMSO-d6) δ 182.69, 147.65, 147.38, 140.58, 137.66, 137.48, 134.67, 131.83, 131.62, 126.90, 125.99, 124.58, 124.48, 122.53, 121.70, 118.91, 116.19, 111.72, 20.64. HRMS (ESI) (positive mode): m/z calculated for $C_{19}H_{13}N_2O$: 285.1024; $(M\text{-}Br)^+$, found: 285.1022.

*9-bromo-13-oxo-12,13-dihydropyrido[1,2-a:3,4-b']diindol-5-ium bromide (**2d**)* Cyclization was conducted at 220 °C for 1 h. Yield: 40%; dark brown solid; m.p. > 300 °C. The solubility of **2d** in common organic solvents is too low to carry out NMR measurement. FTIR (KBr, cm^{-1}): 3428, 3068, 2922, 1722, 1704, 1622, 1598, 1508, 1485, 1472, 1448, 1421, 1401, 1384, 1298, 1276, 1186, 1165, 1125, 1082, 1031, 960, 825, 752, 730, 668, 608, 569, 512, 429. HRMS (ESI) (positive mode): m/z calculated for $C_{18}H_{10}BrN_2O$: 348.9971; $(M\text{-}Br)^+$, found: 348.9962.

*9-carboxy-13-oxo-12,13-dihydropyrido[1,2-a:3,4-b']diindol-5-ium bromide (**2e**)* Cyclization was conducted at 220 °C for 1 h. Yield: 82%; dark brown solid; m.p. > 300 °C. FTIR (KBr, cm^{-1}): 3435, 3090, 1721, 1625, 1576, 1513, 1467, 1420, 1379, 1301, 1280, 1257, 1234, 1187, 1055, 975, 760, 725, 671, 617. ^{1}H NMR (400 MHz, TFA-d) δ 9.36 (s, 1H), 9.29 (d, J = 5.9 Hz, 1H), 9.00 (d, J = 5.9 Hz, 1H), 8.77 (d, J = 8.8 Hz, 1H), 8.27 (d, J = 8.1 Hz, 1H), 8.20 (d, J = 7.4 Hz, 1H), 8.08 (m, 2H), 7.88 (t, J = 7.6 Hz, 1H). ^{13}C NMR (101 MHz, TFA-d) δ 183.06, 171.24, 149.96, 146.96, 142.49, 138.40, 136.38, 133.24, 132.47, 127.52, 127.43, 126.98, 124.61, 123.26, 121.75, 120.85, 119.52, 114.72, 113.75. HRMS (ESI) (positive mode): m/z calculated for $C_{19}H_{11}N_2O_3$: 315.0764; $(M\text{-}Br)^+$, found: 315.0763.

*9-carbamoyl-13-oxo-12,13-dihydropyrido[1,2-a:3,4-b']diindol-5-ium bromide (**2f**)* Cyclization was conducted at 220 °C for 1 h. Yield: 78%; dark brown solid; m.p. > 300 °C. The solubility of **2f** in common organic solvents is too low to carry out NMR measurement. FTIR (KBr, cm^{-1}): 3431, 2647, 1599, 1511, 1385, 1355, 1292, 1221, 1175, 1120, 976, 753. HRMS (ESI) (positive mode): m/z calculated for $C_{19}H_{12}N_3O_2$: 314.0924; $(M\text{-}Br)^+$, found: 314.0920.

*13-oxo-9-(phenylcarbamoyl)-12,13-dihydropyrido[1,2-a:3,4-b']diindol-5-ium bromide (**2g**)* Cyclization was conducted at 220 °C for 1 h. Yield: 82%; dark brown solid; m.p. > 300 °C. ^{1}H NMR (400 MHz, TFA-d) δ 9.24 (s, 1H), 9.20 (d, J = 4.6 Hz, 1H), 9.04 (d, J = 3.9 Hz, 1H), 8.49 (d, J = 8.6 Hz, 1H), 8.19 (d, J = 8.0 Hz, 1H), 8.14 (d, J = 7.4 Hz, 1H), 8.03 (t, J = 8.2 Hz, 2H), 7.82 (t, J = 7.5 Hz, 1H), 7.58 (d, J = 7.7 Hz, 2H), 7.46 (t, J = 7.4 Hz, 2H), 7.36 (t, J = 7.3 Hz, 1H). ^{13}C NMR (101 MHz, TFA-d) δ 182.80, 169.58, 148.97, 146.76, 141.95, 138.17, 134.38, 133.74, 132.97, 132.29, 129.08, 128.97, 127.91, 127.60, 126.79, 126.67, 123.11, 123.08, 121.60, 121.32, 119.48, 114.59, 114.12. HRMS (ESI) (positive mode): m/z calculated for $C_{25}H_{16}N_3O_2$: 390.1237; $(M\text{-}Br)^+$, found:

390.1222.

*9-methyl-13-oxo-12,13-dihydropyrido[1,2-a:3,4-b']diindol-5-ium chloride (**2i**)* Cyclization was conducted at 220 °C for 1 h. Yield: 80%; dark brown solid; m.p. > 300 °C. ^{1}H NMR (500 MHz, Methanol-d4) δ 9.27 (s, 1H), 8.79 (s, 1H), 8.31 (d, J = 8.0 Hz, 1H), 8.12 (s, 1H), 8.02 - 7.94 (m, 2H), 7.74 (t, J = 7.5 Hz, 1H), 7.60 - 7.52 (m, 2H), 2.46 (s, 3H). ^{13}C NMR (126 MHz, MeOD-d4) δ 183.11, 148.61, 147.28, 142.33, 138.49, 137.76, 135.02, 132.96, 132.83, 127.35, 126.94, 125.45, 124.41, 123.05, 121.30, 121.05, 116.62, 114.40, 21.42. HRMS (ESI) (positive mode): m/z calculated for $C_{19}H_{13}N_2O$: 285.1022; $(M\text{-}Cl)^+$, found: 285.1014.

Evaluation of Cholinesterase Activity

The evaluation of cholinesterase activity was conducted following to the method described in a previously study[56]. After the sacrifice of mice, the brains and serum were collected to provide AChE and BuChE, respectively, followed by the addition of 10 times volume of lysis buffer [10 mM HEPES (pH 7.5), 1 mM EGTA, 1 mM EDTA, 150 mM Triton X-100 and 1 mM NaCl; Shanghai Aladdin Biochemical Technology, Shanghai, China]. In order to obtain AChE, the mixture was homogenized on ice and then centrifuged at 3000 rpm at 4 °C for 15 min, and the supernatant was collected. The serum was centrifuged at 13400 rpm at 4 °C for 15 min, and the supernatant was collected to obtain BuChE. Then AChE and BuChE was incubated with 0.1 mM ethopropazine hydrochloride or BW284C51 at 37 °C for 5 min to inhibit BuChE or AChE activity, respectively. Then the test compound was added to the working solution [0.1 M Na_2HPO_4 (pH 7.5), 10 mM DTNB and 1 mM acetylthiocholine iodide (ATCI) for AChE assay or butylthiocholine iodide for BuChE assay (Sigma-Aldrich, St. Louis, MO, USA) followed by pre-incubating with AChE or BuChE at 37 °C for 15 min. Then the substrate (ATCI or butylthiocholine iodide) was added, and incubated at 37 °C for 30 min. AChE and BuChE activity was evaluated by measuring the absorbance at 412 nm using a Varioskan LUX Multimode Microplate Reader (Thermo Fisher Scientific, Waltham, MA, USA).

Molecular Docking Analysis

The X-ray structure of human AChE in complex with donepezil was retrieved from the RCSB protein Data Bank (PDB ID 4EY7)[57]. The drug was analyzed by Molecular Operating Environment. Molecular docking was carried out on Gold 5.2.2 (Cambridge Crystallographic Data Centre Software Ltd., Cambridge, U.K.). The binding pocket was defined by the residues within five angstrom radius of donepezil. The original inhibitor donepezil was removed after defining the binding pocket. A genetic algorithm (GA) and Gold score was used to calculate and select the best docking conformation in the binding pocket.

Cell Culture and Treatment

Human neuroblastoma SH-SY5Y cells were purchased from the Shanghai Institute of Cell Biology (Shanghai, China) and cultured in Dulbecco's modified Eagle's medium (DMEM; Sigma-Aldrich) supplemented with penicillin (100 U/mL), 10 % fetal bovine serum (FBS) and streptomycin (100 μg/mL) in the humidified 5 % CO_2/95 % O_2 atmosphere at 37 °C for 48 h. Then the medium was adjusted to low serum content (1 % FBS) and seeded in 6-well or 96-well plates (around 20000 cells/mL), followed by the cultivation for 48 h. Then SH-SY5Y cells were pre-treated with tested drugs for 1 h followed by exposing to H_2O_2 (0.3 mM) for another 24 h, exclusive of the control.

Measurement of Cell Viability

Cell viability was evaluated by 3(4,5-dimethylthiazol-2-yl)-2,5-diphenylte-trazolium bromide (MTT) assays described in a previous study[58]. Briefly, 10 μL MTT solution (5 mg/mL; Ningbo Baichuan Biotechnology, Ningbo, Zhejiang, China) was added to 6-well or 96-well plates and incubated in the humidified incubator at 37 °C for 4 h. Then 100 μL solvating solution (10 % SDS solution supplemented with 10 mM HCl) was added and incubated silently for 16-20 h. The cell viability was evaluated by measuring the absorbance at 570 nm with 655 nm as a reference wavelength using a Varioskan LUX Multimode Microplate Reader (Thermo Fisher).

FDA/PI Double Staining Assay

FDA/PI double staining was conducted according to the protocol described previously[59]. SH-SY5Y cells were incubated with 10 μg/mL of FDA (Ningbo Baichuan Biotechnology, Zhejiang, China) and 5 μg/mL of PI (Ningbo Baichuan Biotechnology) in 6-well plates for 15 min. After the staining agents were removed, SH-SY5Y cells were washed gently for twice using phosphate buffer. Then UV light microscopy was used to observe and take images of stained cells. Five same-acreage square fields of each well were chosen randomly to count the number of FDA-positive and FDA-negative cells. The cell viability was the ratio of the amount of FDA-positive cells over the total calculated numbers of cells.

Cytokine Determination

The brain was collected immediately after decapitation of mice and then homogenized in 0.5 mL lysis buffer [10 mM HEPES (pH 7.5), 1 mM EGTA, 1 mM EDTA, 0.5% Triton X-100 and 150 mM NaCl; Shanghai Aladdin Biochemical Technology]. The homogenate was then incubated on ice for 1 h, followed by centrifuging at 13400 rpm at 4 °C for 30 min. The concentrations of cytokines (IL-1β, TNF-α, IL-6, IL-10) in the supernatants were measured using ELISA kits (Jiangsu Meibiao Biotechnology, Jiangsu, China) according to the producer's instructions.

Western Blotting Analysis

Western blotting assay was conducted according to a protocol described previously[60]. Hippocampus was collected and weighted immediately after decapitation of mice, followed by the addition of ten

times volume of lysis buffer [10 mM HEPES (pH 7.5), 1 mM EGTA, 1 mM EDTA, 150 mM Triton X-100 and 1 mM NaCl; Shanghai Aladdin Biochemical Technology]. The mixture was then centrifuged at 13400 rpm for 15 min, followed by the measuring of the concentration of protein in the supernatant using BCA Protein Kit (Beyotime Biotechnology, Shanghai, China). The sodium dodecyl sulfate-polyacrylamide gel electrophoresis (SDS-PAGE) was used to electrophorese the protein samples in ice-water mixture at 120 V for 100 min. The separated protein was then transferred to polyvinylidene fluoride membrane using the trans-blotting apparatus at 100 V for 75 min. The membrane was blocked using 5 % skim milk at room temperature (20-25 °C) for 2 h, followed by incubating with primary antibodies against IL-17, ChAT, tau, p-tau and β-actin (Santa Cruz Biotechnology, Santa Cruz, CA, USA) respectively at 4 °C for 12 h. Then the membrane was washed for four times (15 min for each time) using TBST solution (2 mM NaCl, 10 mM Tris-HCl and 0.1 % Tween-20; Shanghai Aladdin Biochemical Technology) followed by incubating with secondary antibodies which specificity bind to the particular primary antibody at room temperature for 1 h. The membrane was washed for four times (15 min for each time) using TBST solution at room temperature. The protein bands were visualized using the ECL Western blotting detection reagents (Amersham Biosciences, Buckingham-shire, UK). The concentrations of proteins were evaluated by analyzing the intensity of each band using Image J software (NIH Image, Bethesda, MD, USA).

Studies on Animals

All animal studies were obeyed the National Institutes of Health (NIH) Guide for the Care and Use of Laboratory Animals (NIH Publications No. 8023, revised 1978) and were approved by the Animal Care and Use Committee of Ningbo University. ICR mice (male, 4-month old, weighted 25 ± 5 g) were purchased from Zhejiang Academy of Sciences (Hangzhou, Zhejiang, China). Mice were fed in a 12 h light/dark cycle under the controlled humidity (50 ± 10%) and temperature (22 ± 2 °C).

Intrahippocampal injection

Mice were anesthetized by *i.p.* administration of 50 mg/kg sodium pentobarbital (Beyotime Biotechnology), and then placed in a stereotaxic instrument (RWD Life Science, Shenzhen, Guangdong, China). After the skull was exposed, two holes were drilled in the skull at the stereotaxic coordinates according to a previous report: anteroposterior -3.8 mm from bregma; mediolateral ± 2 mm from midline; and dorsoventral -3.0 mm from the skull[45]. Then a microinjection needle (Shanghai Gaoge Industrial and Trading Co, LTD, Shanghai, China) was inserted into the hole and 2.0 μL of different doses of **2a**, **2b**, Aβ oligomers or vehicle (saline) were injected into the CA1 region (1.0 μL each side) at a constant speed of 0.2 μL/min using an UltraMicroPump (RWD Life Science). After injection, the needle was left in place for an additional 5 min to facilitate diffusion of the solution away from the needle tip. After the surgery, mice were

given 24 h to recover before animal tests.

Animal treatments

To evaluate the efficacy of **2a** and **2b** in ameliorating scopolamine-induced cognition impairments, donepezil (Santa Cruz Biotechnology), scopolamine (Sigma), **2a** and **2b** were dissolved in sterile saline. Mice were assigned randomly into 7 various groups with 8 animals of each: control (saline), 4mg/kg scopolamine (*i.p.*) plus vehicle, scopolamine plus 4 mg/kg donepezil (*i.p.*), scopolamine plus 70.2 ng **2a** (intrahippocampal injection), scopolamine plus 105.3 ng **2a**(intrahippocampal injection), scopolamine plus 7.3 ng **2b** (intrahippocampal injection) and scopolamine plus 21.9 ng **2b** (intrahippocampal injection). In the scopolamine and control group, mice were intrahippocampal (half of mice) or *i.p.* (half of mice) administrated with the vehicle (saline). Scopolamine was *i.p.* injected 45 min before while donepezil was *i.p.* treated 1 h prior to each animal test for 10 consecutive days. **2a** and **2b** were intrahippocampal injection injected every third day 24 h before each animal test.

When measured the ability of **2a** and **2b** to rescue the learning and memory dysfunctions induced by Aβ oligomers, Aβ was purchased from Sigma, and diluted in sterile saline to the concentration of 60 μM. Mice were assigned randomly into 6 various groups with 8 animals of each: control (saline, intrahippocampal injection), 0.6 μg Aβ oligomers (intrahippocampal injection) plus vehicle, Aβ oligomers plus 70.2 ng **2a** (intrahippocampal injection), Aβ oligomers plus 105.3 ng **2a** (intrahippocampal injection), Aβ oligomers plus 7.3 ng **2b** (intrahippocampal injection) and Aβ oligomers plus 21.9 ng **2b** (intrahippocampal injection). Aβ oligomers were injected 7 days prior to the animal tests, while **2a** and **2b** were intrahippocampal injected every third day 24 h before each animal test. In control and Aβ oligomers group, vehicle (saline) was intrahippocampal injected as the same frequency as **2a** and **2b**.

Open Field Tests

The open field tests were used to evaluate the exploratory and locomotor activities of animals. As described in a previous study, the test was conducted in a 50×50×39 cm open plastic box whose floor was divided in to four equal quadrants by crossed black lines[58]. Mice were placed in the center of the open field and allowed to explore freely for 5 min. The number of rearing (mice stood on their hind legs) and line crossing was recorded. In order to avoid distribution of mice due to the urine and odor, the open field was cleaned between two individual tests using 10 % ethanol.

NOR Tests

The NOR test conducted in a 50×50×39 cm black open plastic box described previously was used to measure the memory function of animals[61]. There were two sessions of the tests, namely training section and exploring session. In the training session, mice were placed in the center of the box and

allowed to explore two identical 5×5×5 cm stone cubes freely for 5 min. The exploring session was conducted after 24 h and one of the stone cube was replaced by a 5×5×7 cm stone square pyramid. The mice were placed in the center of the box and allowed to explore the two different objects freely in the field for 5 min. Mice looked towards and sniffed the object was defined as exploration while sitting on or back on the objects closely was not considered as exploratory behavior. In order to avoid distribution of mice due to the urine and odor, the field was cleaned between two individual tests using 10% ethanol. The recognition index was the ratio of the amount of time spent exploring either of the two identical objects (in the training session) or the novel object (in the exploring session) over the total exploring time (sum of the time spent exploring 2 objects) and was used to evaluate the cognitive function.

MWM Tests

The MWM tests conducted according to a protocol described in a previous study was used to evaluate the spatial learning and memory[62]. The water maze was a circle poor with the diameter of 150 cm and divided into four equal quadrants, and was filled with water at the temperature of 25 °C. A circle platform with the diameter of 5 cm was located in the first quadrant except on the last day and covered by water on the first day only. The camera attached to a computer-based video analyzer was used to monitor the movement of mice. Mice were placed into the water maze at one of the quadrants each time facing the wall and then given 90 s to find the platform, and were allowed to stay on it for 10 s. Mice who failed to reach the platform within 90 s would be guided to the platform gently and allowed to stay on it for 20 s, and they were recorded a escape latency (the time spent escaping onto the submerged platform) of 90 s. Mice were trained to find the platform with four trials per day (mice were placed into different quadrants each trail) for 5 days and the escape latency was recorded. On the 5th day, a probe trial was conducted and the platform was removed, mice were allowed to swim in the poor freely for 90 s. The time of mice spent in the target quadrant (the first quadrant) and number of platform region crossing was recorded in order to evaluate the spatial recognition function.

Y Maze Tests

The Y maze tests were conducted in a 30×8×30 cm black open box with three identical arms described previously[63]. Different geometric figures were attached to particular arm as visual markers. Three arms were randomly assigned as the new arm and two other arms, and the junction was defined as central area. The tests consisted of namely training and exploring session with an interval of 2 h. In the training session, the new arm was blocked by a partition. Mice were put into the central area and allowed to explore freely in the box except the new arm for 5 min. In the exploring session, the baffle was removed. Mice were put into the central area and allowed to explore freely in the box for 5 min. The movement of mice was monitored by a video attached to a trajectory tracking system and the time of mice spent in each arms was recorded. The spontaneous alteration was the ratio of

the amount of time spent exploring the new arm over the total exploring time (sum of the time spent exploring three arms) and was used to evaluate cognitive function.

Statistical Analysis

The results were presented as mean ± SD for n = 8 mice/group. GraphPad Prism (version 6.0, GraphPad Software, Inc., San Diego, CA, USA) was used to analyze the data. The group differences were evaluated using one-way analysis of variation (ANOVA) and Tukey's test was used for the statistical comparison. However, two-way ANOVA with the repeated measure of both the factor of treatment and training day was used to analyze the group variance of the escape latency in the training days (1^{th}-5^{th} day) of Morris water maze. Values of $p < 0.05$ were considered statistically significant. In figures, % or folds of control was calculated by separating each control mice value on the average of total control group values for a particular cytokine protein or protein and then the values of treated group were normalized to control (1.0).

Associated Content

Supporting Information

Representative ^{1}H NMR and ^{13}C NMR spectra and HPLC analysis of synthesized compounds; Pharmacokinetics studies of compound **2b**.

Author Information

Corresponding Authors

*Hongze Liang, Email: lianghongze@nbu.edu.cn.

*Wei Cui, Email: cuiwei@nbu.edu.cn.

ORCID

Hongze Liang: 0000-0002-8278-2258

Wei Cui: 0000-0002-8645-4278

Hanbo Pan: 0000-0001-5880-2573

Author Contributions

Wei Cui, Hongze Liang, Xiaojun Yan and Fufeng Liu designed the study, Wei Cui, Hongze Liang and Hanbo Pan drafted the manuscript; Hongda Qiu, Miaoman Lin, Ming He, Weida Liang, Yongmei Li performed chemistry; Ke Zhang, Mengxiang Yang, Chenye Mou and Xiao Xiao performed AChE inhibition assay and H_2O_2-induced neuronal death model; Haixiao Jin performed molecular docking; Hanbo Pan, Panpan Zhang, Difan Zhang and Haixing Wang performed animal studies and biochemical testing; All authors read and approved the final manuscript.

Acknowledgements

This research was funded by the National Natural Science Foundation of China (81870853, 21878234, 20903058), Ningbo Sci & Tech Project for Common Wealth (2017C50042), Zhejiang Key Laboratory of Pathophysiology (201804), Open Project Program of State Key Laboratory of Food Nutrition and Safety, Tianjin University of Science & Technology (SKLFNS-KF-201806), Ningbo municipal innovation team of life science and health (2015C110026), the 111 Project (D16013), Li Dak Sum Marine Biopharmaceutical Development Fund, and the K. C. Wong Magna Fund in Ningbo University.

Competing Interests

The authors declare that they have no competing interests.

References

(1) Chen, H. X.; Xiang, S. Y.; Huang, L.; Lin, J. J.; Hu, S. Q.; Mak, S. H.; Wang, C.; Wang, Q. W.; Cui, W.; Han, Y. F. Tacrine(10)-Hupyridone, a Dual-Binding Acetylcholinesterase Inhibitor, Potently Attenuates Scopolamine-Induced Impairments of Cognition in Mice. *Metab. Brain. Dis.* **2018**, *33* (4), 1131-1139.

(2) Wang, J. L.; Zheng, J. C.; Huang, C. H.; Zhao, J. Y.; Lin, J. J.; Zhou, X.; Naman, C.B.; Wang, N.; Gerwick, W.H.; Wang, Q. W.; Yan, X. J.; Cui, W.; He, S. Eckmaxol, a Phlorotannin Extracted from Ecklonia Maxima, Produces Anti-B-Amyloid Oligomer Neuroprotective Effects Possibly Via Directly Acting on Glycogen Synthase Kinase 3β. *ACS. Chem. Neurosci.* **2018**, *9* (6), 1349-1356.

(3) Jing, L.; Wu, G.; Kang, D.; Zhou, Z.; Song, Y.; Liu, X.; Zhan, P. Contemporary Medicinal-Chemistry Strategies for the Discovery of Selective Butyrylcholinesterase Inhibitors. *Drug Discov. Today.* **2019**, *24* (2), 629-635.

(4) Wang, W.; Yang, Y.; Ying, C.; Li, W.; Ruan, H.; Zhu, X.; You, Y.; Han, Y.; Chen, R.; Wang, Y.; Li, M. Inhibition of Glycogen Synthase Kinase-3β Protects Dopaminergic Neurons from Mptp Toxicity. *Neuropharmacology.* **2007**, *52* (8), 1678-1684.

(5) Xian, Y. F.; Ip, S. P.; Mao, Q. Q.; Su, Z. R.; Chen, J. N.; Lai, X. P.; Lin, Z. X. Honokiol Improves Learning and Memory Impairments Induced by Scopolamine in Mice. *Eur. J. Pharmacol.* **2015**, *760*, 88-95.

(6) Wang, D. P.; Yin, H.; Lin, Q.; Fang, S. P.; Shen, J. H.; Wu, Y. F.; Su, S. H.; Hai, J. Andrographolide Enhances Hippocampal Bdnf Signaling and Suppresses Neuronal Apoptosis, Astroglial Activation, Neuroinflammation, and Spatial Memory Deficits in a Rat Model of Chronic Cerebral Hypoperfusion. *Naunyn Schmiedebergs Arch. Pharmacol.* **2019**, *392* (10), 1277-1284.

(7) Akiyama, H.; Barger, S.; Barnum, S.; Bradt, B.; Bauer, J.; Cole, G. M.; Cooper, N. R.; Eikelenboom, P.; Emmerling, M.; Fiebich, B. L.; Finch, C. E.; Frautschy, S.; Griffin, W. S. T.; Hampel, H.; Hull, M.; Landreth, G.; Lue, L. F.; Mrak, R.; Mackenzie, I. R.; McGeer, P. L.; O'Banion, M. K.; Pachter, J.; Pasinetti, G.; Plata–Salaman, C.; Rogers, J.; Rydel, R.; Shen, Y.; Streit, W.; Strohmeyer, R.; Tooyoma, I.; Van Muiswinkel, F. L.; Veerhuis, R.; Walker, D.; Webster, S.; Wegrzyniak, B.; Wenk, G.; Wyss-Coray, T. Inflammation and Alzheimer's Disease. *Neurobiol. Aging.* **2000**, *21* (3), 383-421.

(8) Kawarabayashi, T.; Terakawa, T.; Takahashi, A.; Hasegawa, H.; Narita, S.; Sato, K.; Nakamura, T.; Seino, Y.; Hirohata, M.; Baba, N.; Ueda, T.; Harigaya, Y.; Kametani, F.; Maruyama, N.; Ishimoto, M.; St George-Hyslop, P.; Shoji, M. Oral Immunization with Soybean Storage Protein Containing Amyloid-Beta 4-10 Prevents Spatial Learning Decline. *J. Alzheimers Dis.* **2019**, *70* (2),

487-503.

(9) Yang, Y.; Giau, V. V.; An, S. S. A.; Kim, S. Plasma Oligomeric Beta Amyloid in Alzheimer's Disease with History of Agent Orange Exposure. *Dement. Neurocogn. Disord.* **2018**, *17* (2), 41-49.

(10) Bayart, J. L.; Hanseeuw, B.; Ivanoiu, A.; van Pesch, V. Analytical and Clinical Performances of the Automated Lumipulse Cerebrospinal Fluid Aβ42 and T-Tau Assays for Alzheimer's Disease Diagnosis. *J. Neurol.* **2019**, *266* (9), 2304-2311.

(11) Chen, D. L.; Drombosky, K. W.; Hou, Z. Q.; Sari, L.; Kashmer, O. M.; Ryder, B. D.; Perez, V. A.; Woodard, D. R.; Lin, M. M.; Diamond, M. I.; Joachimiak, L. A. Tau Local Structure Shields an Amyloid-Forming Motif and Controls Aggregation Propensity. *Nat. Commun.* **2019**, *10* (1), 2493-2506.

(12) Tripathi, P. N.; Srivastava, P.; Sharma, P.; Tripathi, M. K.; Seth, A.; Tripathi, A.; Rai, S. N.; Singh, S. P.; Shrivastava, S. K. Biphenyl-3-Oxo-1,2,4-Triazine Linked Piperazine Derivatives as Potential Cholinesterase Inhibitors with Anti-Oxidant Property to Improve the Learning and Memory. *Bioorg. Chem.* **2019**, *85*, 82-96.

(13) Morozova, V.; Cohen, L. S.; Makki, A. E.; Shur, A.; Pilar, G. E.; Idrissi, A.; Alonso, A. D. Normal and Pathological Tau Uptake Mediated by M1/M3 Muscarinic Receptors Promotes Opposite Neuronal Changes. *Front. Cell. Neurosci.* **2019**, *13*, 403-414.

(14) Scipioni, M.; Kay, G.; Megson, I. L.; Kong, Thoo, Lin, P. Synthesis of Novel Vanillin Derivatives: Novel Multi-targeted Scaffold Ligands Against Alzheimer's disease. *Medchemcomm.* **2019**, *10* (5), 764-777.

(15) González, J. F.; Alcántara, A. R.; Doadrio, A. L.; Sánchez-Montero, J. M. Developments with Multi-Target Drugs for Alzheimer's Disease: An Overview of the Current Discovery Approaches. *Expert Opin Drug Discov.* **2019**, *14* (9), 879-891.

(16) Batool, A.; Kamal, M. A.; Rizvi, S. M. D.; Rashid, S. Topical Discoveries on Multi-Target Approach to Manage Alzheimer's Disease. *Curr. Drug Metab.* **2018**, 19 *(8),* 704-713.

(17) Manda, S.; Sharma, S.; Wani, A.; Joshi, P.; Kumar, V.; Guru, S. K.; Bharate, S. S.; Bhushan, S.; Vishwakarma, R. A.; Kumar, A.; Bharate, S. B. Discovery of a Marine-Derived Bis-Indole Alkaloid Fascaplysin, as a New Class of Potent P-Glycoprotein Inducer and Establishment of Its Structure-Activity Relationship. *Eur. J. Med. Chem.* **2016**, *107*, 1-11.

(18) Yang, H.; Zhao, X.; Zhao, L.; Liu, L.; Li, J.; Jia, W.; Liu, J.; Huang, G. Prmt5 Competitively Binds to Cdk4 to Promote G1-S Transition Upon Glucose Induction in Hepatocellular Carcinoma. *Oncotarget.* **2016**, *7* (44), 72131-72147.

(19) Chen, S.; Guan, X.; Wang, L. L.; Li, B.; Sang, X. B.; Liu, Y.; Zhao, Y. Fascaplysin Inhibit

Ovarian Cancer Cell Proliferation and Metastasis through Inhibiting Cdk4. *Gene.* **2017**, *635*, 3-8.

(20) Mischitelli, M.; Jemaa, M.; Almasry, M.; Faggio, C.; Lang, F. Triggering of Suicidal Erythrocyte Death by Fascaplysin. *Cell Physiol. Biochem.* **2016**, *39* (4), 1638-1647.

(21) Bharate, S. B.; Manda, S.; Joshi, P.; Singh, B.; Vishwakarma, R. A. Total Synthesis and Anti-Cholinesterase Activity of Marine-Derived Bis-Indole Alkaloid Fascaplysin. *Med. Chem. Comm.* **2012**, *3* (9), 1098-1103.

(22) Sun, Q. M.; Liu, F. F.; Sang, J. C.; Lin, M. M.; Ma, J. L.; Xiao, X.; Yan, S. C.; Naman, C. B.; Wang, N.; He, S.; Yan, X. J.; Cui, W.; Liang, H. Z. 9-Methylfascaplysin Is a More Potent a Aggregation Inhibitor Than the Marine-Derived Alkaloid, Fascaplysin, and Produces Nanomolar Neuroprotective Effects in SH-SY5Y Cells. *Mar. Drugs.* **2019**, *17* (2), 15.

(23) Bellingham, M. C. A Review of the Neural Mechanisms of Action and Clinical Efficiency of Riluzole in Treating Amyotrophic Lateral Sclerosis: What Have We Learned in the Last Decade? *CNS Neurosci. Ther.* **2011**, *17* (1), 4-31.

(24) Stoy, N.; Mackay, G. M.; Forrest, C. M.; Christofides, J.; Egerton, M.; Stone, T.W.; Darlington, L. G. Tryptophan Metabolism and Oxidative Stress in Patients with Huntington's Disease. *J. Neurochem.* **2005**, *93* (3), 611-623.

(25) Choi, J.; Sullards, M. C.; Olzmann, J. A.; Rees, H. D.; Weintraub, S. T.; Bostwick, D. E.; Gearing, M.; Levey, A. I.; Chin, L. S.; Li, L. Oxidative Damage of Dj-1 Is Linked to Sporadic Parkinson and Alzheimer Diseases. *J. Biol. Chem.* **2006**, *281* (16), 10816-10824.

(26) Klinkenberg, I.; Blokland, A. The Validity of Scopolamine as a Pharmacological Model for Cognitive Impairment: A Review of Animal Behavioral Studies. *Neurosci. Biobehav. Rev.* **2010**, *34* (8), 1307-1350.

(27) Chen, L. P.; Huang, C. H.; Shentu, J. Y.; Wang, M. J.; Yan, S. C.; Zhou, F.; Zhang, Z.; Wang, C.; Han, Y. F.; Wang, Q. W.; Cui, W. Indirubin Derivative 7-Bromoindirubin-3-Oxime (7bio) Attenuates Aβ Oligomer-Induced Cognitive Impairments in Mice. *Front. Mol. Neurosci.* **2017**, *10*, 393-407.

(28) Battini, N.; Padala, A. K.; Mupparapu, N.; Vishwakarma, R. A.; Ahmed, Q. N. Unexplored Reactivity of 2-Oxoaldehydes Towards Pictet–Spengler Conditions: Concise Approach to B-Carboline Based Marine Natural Products. *RSC Advances.* **2014**, *4* (50), 26258-26263.

(29) Zhu, Y. P.; Liu, M. C.; Cai, Q.; Jia, F. C.; Wu, A. X. A Cascade Coupling Strategy for One-Pot Total Synthesis of B-Carboline and Isoquinoline-Containing Natural Products and Derivatives. *Chemistry.* **2013**, *19* (31), 10132-10137.

(30) Qiu, H. D.; Liang, W. D.; Zhang, G. J.; Lin, M. M.; Liu, W.; Gao, Z.; Wei, W.; Tang, C. L.;

Jin, H. X.; Liang, H. Z.; Yan, X. J. Aerobic Oxidation of Methyl-Substituted B-Carbolines Catalyzed by N-Hydroxyphthalimide and Metal Catalyst. *ChemistrySelect.* **2018**, *3* (43), 12363-12366.

(31) Li, S. P.; Wang, Y. W.; Qi, S. L.; Zhang, Y. P.; Deng, G.; Ding, W. Z.; Ma, C.; Lin, Q. Y.; Guan, H. D.; Liu, W.; Cheng, X. M.; Wang, C. H. Analogous B-Carboline Alkaloids Harmaline and Harmine Ameliorate Scopolamine-Induced Cognition Dysfunction by Attenuating Acetylcholinesterase Activity, Oxidative Stress, and Inflammation in Mice. *Front. Pharmacol.* **2018**, *9*, 346-361.

(32) Chen, H. X.; Wu, X.; Gu, X. M.; Zhou, Y. Y.; Ye, L. Y.; Zhang, K.; Pan, H. B.; Wang, J. L.; Wei, H.; Zhu, B. B.; Naman, C.B.; Mak, S.; Carlier, P. R.; Cui, W.; Han, Y. F. Tacrine(10)-Hupyridone Prevents Post-Operative Cognitive Dysfunction Via the Activation of Bdnf Pathway and the Inhibition of Ache in Aged Mice. *Front. Cell. Neurosci.* **2018**, *12*, 396-406.

(33) Filali, I.; Romdhane, A.; Znati, M.; B. Jannet, H.; Bouajila, J. Synthesis of New Harmine Isoxazoles and Evaluation of Their Potential Anti-Alzheimer, Anti-Inflammatory, and Anticancer Activities. *Med. Chem.* **2016**, *12* (2), 184-190.

(34) Zhao, Y.; Ye, F.; Xu, J.; Liao, Q.; Chen, L.; Zhang, W.; Sun, H.; Liu, W.; Feng, F.; Qu, W. Design, Synthesis and Evaluation of Novel Bivalent B-Carboline Derivatives as Multifunctional Agents for the Treatment of Alzheimer's Disease. *Biorg. Med. Chem.* **2018**, *26* (13), 3812-3824.

(35) Yu, J.; Lin, J. J.; Yu, R.; He, S.; Wang, Q. W.; Cui, W.; Zhang, J. R. Fucoxanthin Prevents H_2O_2-Induced Neuronal Apoptosis Via Concurrently Activating the Pi3-K/Akt Cascade and Inhibiting the Erk Pathway. *Food. Nutr. Res.* **2017**, *61* (1), 1304678-1304687.

(36) Greda, A.; Jantas, D. Mitochondrial Dysfunctions in Neurodegenerative Diseases: Potential Target for Neuroprotective Drugs. *Postepy. Biologii. Komorki.* **2012**, *39* (3), 321-344.

(37) Spilovska, K.; Korabecny, J.; Nepovimova, E.; Dolezal, R.; Mezeiova, E.; Soukup, O.; Kuca, K. Multitarget Tacrine Hybrids with Neuroprotective Properties to Confront Alzheimer's Disease. *Curr. Top. Med. Chem.* **2017**, *17* (9), 1006-1026.

(38) Vandenberg, L. N.; Wadia, P. R.; Schaeberle, C. M.; Rubin, B. S.; Sonnenschein, C.; Soto, A. M. The Mammary Gland Response to Estradiol: Monotonic at the Cellular Level, Non-Monotonic at the Tissue-Level of Organization? *J. Steroid Biochem. Mol. Biol.* **2006**, *101* (4), 263-274.

(39) McGovern, S. L.; Caselli, E.; Grigorieff, N.; Shoichet, B. K. A Common Mechanism Underlying Promiscuous Inhibitors from Virtual and High-Throughput Screening. *J. Med. Chem.* **2002**, *45* (8), 1712-1722.

(40) Owen, S. C.; Doak, A. K.; Ganesh, A. N.; Nedyalkova, L.; McLaughlin, C. K.; Shoichet, B.

K.; Shoichet, M. S. Colloidal Drug Formulations Can Explain "Bell-Shaped" Concentration–Response Curves. *ACS Chem. Biol.* **2014**, *9* (3), 777-784.

(41) Colovic, M. B.; Krstic, D. Z.; Lazarevic-Pasti, T. D.; Bondzic, A. M.; Vasic, V. M. Acetylcholinesterase Inhibitors: Pharmacology and Toxicology. *Curr. Neuropharmacol.* **2013**, *11* (3), 315-335.

(42) Coll, R. C.; Robertson, A. A. B.; Chae, J. J.; Higgins, S. C.; Muñoz-Planillo, R.; Inserra, M. C.; Vetter, I.; Dungan, L. S.; Monks, B. G.; Stutz, A.; Croker, D. E.; Butler, M. S.; Haneklaus, M.; Sutton, C. E.; Núñez, G.; Latz, E.; Kastner, D. L.; Mills, K. H. G.; Masters, S. L.; Schroder, K.; Cooper, M.A.; O'Neill, L. A. J. A Small-Molecule Inhibitor of the Nlrp3 Inflammasome for the Treatment of Inflammatory Diseases. *Nat. Med.* **2015**, *21* (3), 248-55.

(43) Muhammad, T.; Ali, T.; Ikram, M.; Khan, A.; Alam, S. I.; Kim, M. O. Melatonin Rescue Oxidative Stress-Mediated Neuroinflammation/Neurodegeneration and Memory Impairment in Scopolamine-Induced Amnesia Mice Model. *J. Neuroimmune. Pharmacol.* **2019**, *14* (2), 278-294.

(44) Zambrano, P.; Suwalsky, M.; Jemiola-Rzeminska, M.; Strzalka, K.; Sepúlveda, B.; Gallardo M. J.; Aguilar L. F. The Acetylcholinesterase (AChE) Inhibitor and Anti-Alzheimer Drug Donepezil Interacts with Human Erythrocytes. *Biochim. Biophys. Acta Biomembr.* **2019**, *1861* (6), 1078-1085.

(45) Eskandary, A.; Moazedi, A. A.; Najaph Zade, H.; Akhond, M. R. Effects of Donepezil Hydrochloride on Neuronal Response of Pyramidal Neurons of the CA1 Hippocampus in Rat Model of Alzheimer's Disease. *Basic. Clin. Neurosci.* **2019**, *10* (2), 109-117.

(46) Duma, C.; Kopyov, O.; Kopyov, A.; Berman, M.; Lander, E.; Elam, M.; Arata, M.; Weiland, D.; Cannell, R.; Caraway, C.; Berman, S.; Scord, K.; Stemler, L.; Chung, K.; Khoudari, S.; McRory, R.; Duma, C.; Farmer, S.; Bravo, A.; Yassa, C.; Sanathara, A.; Singh, E.; Rapaport, B. Human Intracerebroventricular (Icv) Injection of Autologous, Non-Engineered, Adipose-Derived Stromal Vascular Fraction (Adsvf) for Neurodegenerative Disorders: Results of a 3-Year Phase 1 Study of 113 Injections in 31 Patients. *Mol. Biol. Rep.* **2019**, *46* (5), 5257-5272.

(47) Zarei, M.; Mohammadi, S.; Jabbari, S.; Shahidi, S. Intracerebroventricular Microinjection of Kaempferol on Memory Retention of Passive Avoidance Learning in Rats: Involvement of Cholinergic Mechanism(S). *Int. J. Neurosci.* **2019**, *129* (12), 1203-1212.

(48) Ravelli, K. G.; Rosário, B. D. A.; Camarini, R.; Hernandes, M. S.; Britto, L. R. Intracerebroventricular Streptozotocin as a Model of Alzheimer's Disease: Neurochemical and Behavioral Characterization in Mice. *Neurotox. Res.* **2017**, *31* (3), 327-333.

(49) Wang, D.; Hu, M.; Li, X.; Zhang, D.; Chen, C.; Fu, J.; Shao, S.; Shi, G.; Zhou, Y.; Wu, S.; Zhang, T. Design, Synthesis, and Evaluation of Isoflavone Analogs as Multifunctional Agents for

the Treatment of Alzheimer's Disease. *Eur. J. Med. Chem.* **2019**, *168*, 207-220.

(50) Barai, P.; Raval, N.; Acharya, S.; Borisa, A.; Bhatt, H.; Acharya, N. Neuroprotective Effects of Bergenin in Alzheimer's Disease: Investigation through Molecular Docking, in Vitro and in Vivo Studies. *Behav. Brain. Res.* **2019**, *356*, 18-40.

(51) Heneka, M. T.; Kummer, M. P.; Stutz, A.; Delekate, A.; Schwartz, S.; Vieira-Saecker, A.; Griep, A.; Axt, D.; Remus, A.; Tzeng, T. C.; Gelpi, E.; Halle, A.; Korte, M.; Latz, E.; Golenbock, D. T. Nlrp3 Is Activated in Alzheimer's Disease and Contributes to Pathology in App/Ps1 Mice. *Nature.* **2013**, *493* (7434), 674-678.

(52) Jia, L.; Sun, P.; Gao, H.; Shen, J.; Gao, Y.; Meng, C.; Fu, S. D.; Yao, H. J.; Zhang, G. Mangiferin Attenuates Bleomycin-Induced Pulmonary Fibrosis in Mice through Inhibiting Tlr4/P65 and Tgf-Beta 1/Smad2/3 Pathway. *J. Pharm. Pharmacol.* **2019**, *71* (6), 1017-1028.

(53) Huang, W.; Liang, M.; Li, Q.; Zheng, X.; Zhang, C.; Wang, Q.; Tang, L.; Zhang, Z.; Wang, B.; Shen, Z. Development of the "Hidden" Multifunctional Agents for Alzheimer's Disease. *Eur. J. Med. Chem.* **2019**, *177*, 247-258.

(54) Fu, W.; Vukojevic, V.; Patel, A.; Soudy, R.; MacTavish, D.; Westaway, D.; Kaur, K.; Goncharuk, V.; Jhamandas, J. Role of Microglial Amylin Receptors in Mediating Beta Amyloid (Aβ)-Induced Inflammation. *J Neuroinflammation.* **2017**, *14* (1), 199-211.

(55) Yan, X.; Chen, H.; Lu, X.; Wang, F.; Xu, W.; Jin, H.; Zhu, P. Fascaplysin Exert Anti-Tumor Effects through Apoptotic and Anti-Angiogenesis Pathways in Sarcoma Mice Model. *Eur. J. Pharm. Sci.* **2011**, *43* (4), 251-259.

(56) Xian, Y. F.; Lin, Z. X.; Zhao, M.; Mao, Q. Q.; Ip, S. P.; Che, C. T. Uncaria Rhynchophylla Ameliorates Cognitive Deficits Induced by D-Galactose in Mice. *Planta. Med.* **2011**, *77* (18), 1977-1983.

(57) Cheung, J.; Rudolph, M. J.; Burshteyn, F.; Cassidy, M. S.; Gary, E. N.; Love, J.; Franklin, M.C.; Height, J. J. Structures of Human Acetylcholinesterase in Complex with Pharmacologically Important Ligands. *J. Med. Chem.* **2012**, *55* (22), 10282-10286.

(58) Modarresi, M.; Hajialyani, M.; Moasefi, N.; Ahmadi, F.; Hosseinzadeh, L. Evaluation of the Cytotoxic and Apoptogenic Effects of Glabridin and Its Effect on Cytotoxicity and Apoptosis Induced by Doxorubicin Toward Cancerous Cells. *Adv. Pharm. Bull.* **2019**, *9* (3), 481-489.

(59) Lin, J. J.; Mak, S. H.; Zheng, J. C.; Wang, J. L.; Xu, D. L.; Hu, S. Q.; Zhang, Z. J.; Wang, Q. W.; Han, Y. F.; Cui, W. Assessment of Neuronal Viability Using Fluorescein Diacetate-Propidium Iodide Double Staining in Cerebellar Granule Neuron Culture. *J. Vis. Exp.* **2017**, *123*, 55442-55448.

(60) Cui, W.; Zhang, Z. J.; Hu, S. Q.; Mak, S. H.; Xu, D. P.; Choi, C. L.; Wang, Y. Q.; Tsim, W.

K.; Lee, M. Y.; Rong, J. H.; Han, Y. F. Sunitinib Produces Neuroprotective Effect Via Inhibiting Nitric Oxide Overproduction. *CNS Neurosci. Ther.* **2014**, *20* (3), 244-252.

(61) Lu, Y.; Wang, C.; Xue, Z. C.; Li, C. L.; Zhang, J. F.; Zhao, X.; Liu, A. M.; Wang, Q. W.; Zhou, W. H. Pi3k/Akt/Mtor Signaling-Mediated Neuropeptide Vgf in the Hippocampus of Mice Is Involved in the Rapid Onset Antidepressant-Like Effects of Glyx-13. *Int. J. Neuropsychopharmacol.* **2015**, *18* (5), 12-23.

(62) Chang, L.; Cui, W.; Yang, Y.; Xu, S.; Zhou, W.; Fu, H.; Hu, S.; Mak, S.; Hu, J.; Wang, Q.; Ma, V. P.; Choi, T. C.; Ma, E. D.; Tao, L.; Pang, Y.; Rowan, M. J.; Anwyl, R.; Han, Y.; Wang, Q. Protection against Beta-Amyloid-Induced Synaptic and Memory Impairments Via Altering Beta-Amyloid Assembly by Bis(Heptyl)-Cognitin. *Sci. Rep.* **2015**, *5*, 10256-10271.

(63) Sohn, E.; Lim, H. S.; Kim, Y. J.; Kim, B. Y.; Kim, J. H.; Jeong, S. J. Elaeagnus Glabra F. Oxyphylla Attenuates Scopolamine-Induced Learning and Memory Impairments in Mice by Improving Cholinergic Transmission Via Activation of Creb/Ngf Signaling. *Nutrients.* **2019**, *11* (6), 1205-1218.

Figure captions

Figure 1 Synthesis routs of β-carboline and fascaplysin derivatives. (A) Synthesis of compounds **1a**-**1e**, **1h**-**1i** and **2a**-**2e**, **2h**-**2i**. (B) Synthesis of compounds **1f**-**1g**, **1j**-**1k** and **2f**-**2g**. Reagents and conditions: (i) I_2, DMSO, reflux; (ii) 220-230 °C, 20-80 min; (iii) O_2, N-hydroxyphthalimide, $Co(OAc)_2$, room temperature; (iv) $SOCl_2$, Et_3N, THF, reflux, 2 h; amine, THF, room temperature, 12 h. Reagents and conditions: (v) $LiAlH_4$, THF, reflux, 8 h.

Figure 2 *In vitro* AChE inhibition properties and neuroprotection of fascaplysin derivatives. (A) AChE activity was evaluated in a system with or without 0.2 and 0.8 μM **2b**. The concentrations of ATCI were within the scope of 5 to 30 μM. Lineweaver–Burk plot was used to fit 1/[V] *versus* 1/[S]. Every point is an average of three independent experiments. (B) The slopes were calculated from (A). The value of K*i* was calculated by the slopes and concentrations of **2b**. Molecular docking analysis was used to explore the interactions between fascaplysin derivatives and AChE. (C) **2b** (red) bound to the CAS and the PAS of AChE (grey). (D) **2c** (yellow) bound to the CAS and the PAS of AChE (grey). (E) **2d** (blue) bound to the CAS and the PAS of AChE (grey). The electron-withdrawing substituted bromine in **2d** had electron repulsion with aromatic ring of Trp86 in CAS. (F) **2e** (orange) bound to the CAS and the PAS of AChE (grey). The negative charged carboxyl in **2e** had electron repulsion with aromatic ring of Trp86 in CAS. (G) SH-SY5Y cells were incubated with drugs for 1 h, then H_2O_2 were added 24 h before the MTT assay. **2a**, **2b**, **2d**, fucoxanthin (Fuco), tacrine (Tac) and curcumin (Cur) could protect SY-SH5Y cells against H_2O_2-induced neurotoxicity while **2c** and **2e** did not exhibit neuroprotective ability. (H) SH-SY5Y cells were pre-incubated with 3 nM **2b** for 1 h followed by adding 0.3 mM H_2O_2. After incubated for 24 h, the cells were stained by the FDA/PI double staining assay. FDA positive cells (green stained cells) were living cells, while FDA negative cells (red stained cells) were dead cells. (I) Quantitative results demonstrated that treatment with 3 nM **2b** significantly increased the percentage of FDA positive cells meanwhile decreased the percentage of FDA negative cells. Data are expressed as the mean ± SD (n = 6); $^{\#\#}p < 0.01$ *versus* the control group, $^{*}p < 0.05$ and $^{**}p < 0.01$ *versus* the H_2O_2-treated group (One-way ANOVA, Tukey's test).

Figure 3 **2a** and **2b** prevent scopolamine-induced cognitive impairments in mice. In open field tests, **2a** and **2b** treatment did not significantly alter (A) the number of line crossing, and (B) the number of rearing. In NOR tests, **2a** and **2b** treatment (C) did not significantly alter recognition index for two identical objects in the training session, (D) while significantly increased recognition index in the exploring session in scopolamine-treated mice. In MWM tests, **2a** and **2b** treatment (E) significantly decreased the mean latency to find the platform in the training session, (F) and increased the number of target crossings in probe trial in scopolamine-treated mice. (G) Treatment with **2b** could significantly increase the time spent in target quadrant in probe trial in scopolamine-treated mice. (H) Representative paths of mice in the training session of Morris water maze tests. *:

70.2 ng, #: 105.3 ng, $: 7.3 ng, &: 21.9 ng, *i.p.*: intraperitoneal injection, *i.h.p.*: intrahippocampal injection. Data are expressed as the mean ± SD (n = 8); $^{\#\#}p < 0.05$ and $^{\#\#}p < 0.01$ *versus* the control group, $^{*}p < 0.05$ and $^{**}p < 0.01$ *versus* the scopolamine-treated group (one-way ANOVA and Tukey's test).

Figure 4 2a and **2b** prevent scopolamine-induced cholinergic dysfunction and neuroinflammation in mice. (A) AChE activity in hippocampus was measured by AChE activity evaluation assay. **2a** and **2b** treatment could significantly inhibit AChE activity in the hippocampus of scopolamine-treated mice. (B) Western blot analysis of ChAT and β-actin levels in hippocampus. (C) Quantitative results demonstrated that treatment with **2a** at 105.3 ng significantly increased the expressions of ChAT in the hippocampus of scopolamine-treated mice. (D) Western blotting analysis of ChAT and β-actin levels in hippocampus. (E) Quantitative results demonstrated that treatment with **2b** at 21.9 ng significantly increased the expressions of ChAT in the hippocampus of scopolamine-treated mice. The result of EILSA proved that **2a** and **2b** treatment could significantly decrease (F) IL-1β, (G) TNF-α and (H) IL-6 levels while increase (I) IL-10 level in the hippocampus of scopolamine-treated mice. (J) Western blotting analysis of IL-17 and β-actin levels in hippocampus. (K) Quantitative results demonstrated that **2a** at 105.3 ng significantly decreased the expressions of IL-17 in the hippocampus of scopolamine-treated mice. (L) Western blotting analysis of IL-17 and β-actin levels in hippocampus. (M) Quantitative results demonstrated that **2b** at 21.9 ng significantly decreased the expressions of IL-17 in the hippocampus of scopolamine-treated mice. *i.p.*: intraperitoneal injection, *i.h.p.*: intrahippocampal injection. Data are expressed as the mean ± SD (n = 8); $^{\#\#}p < 0.05$ and $^{\#\#}p < 0.01$ *versus* the control group, $^{*}p < 0.05$ and $^{**}p < 0.01$ *versus* the scopolamine-treated group (one-way ANOVA and Tukey's test).

Figure 5 2a and **2b** prevent Aβ oligomers-induced cognitive impairments and tau hyper-phosphorylation in mice. (A) In the exploring session of Y-maze tests, **2a** and **2b** treatment significantly increased the spontaneous alteration in Aβ-treated mice. In NOR tests, **2a** and **2b** treatment (B) did not significantly alter recognition index for two identical objects in the training session, while (C) significantly increased recognition index in the exploring session in Aβ-treated mice. In MMW tests, **2a** and **2b** treatment (D) significantly decreased the mean latency to find the platform in the training session, and (E) increased the time spent in the target quadrant in probe trial in Aβ-treated mice. (F) Representative paths of mice in the training session of MWM tests. The expression of (G) tau, (H) p-tau and β-actin were detected by Western blotting assay. (I) Quantitative results demonstrated that treatment with **2a** significantly decreased p-tau levels in the hippocampus of Aβ-treated mice. Western blotting analysis of (J) tau, (K) p-tau and β-actin levels in hippocampus. (L) Quantitative results demonstrated that treatment with **2b** significantly decreased p-tau levels in the hippocampus of scopolamine-treated mice. *: 70.2 ng, #: 105.3 ng, $: 7.3 ng, &: 21.9 ng, *i.h.p.*: intrahippocampal injection. Data are expressed as the mean ± SD (n = 8); $^{\#\#}p < 0.05$ and $^{\#\#}p < 0.01$

versus the control group, $^{*}p$ <0.05 and $^{**}p$ < 0.01 *versus* the Aβ-treated group (one way ANOVA and Tukey's test).

Figure 1

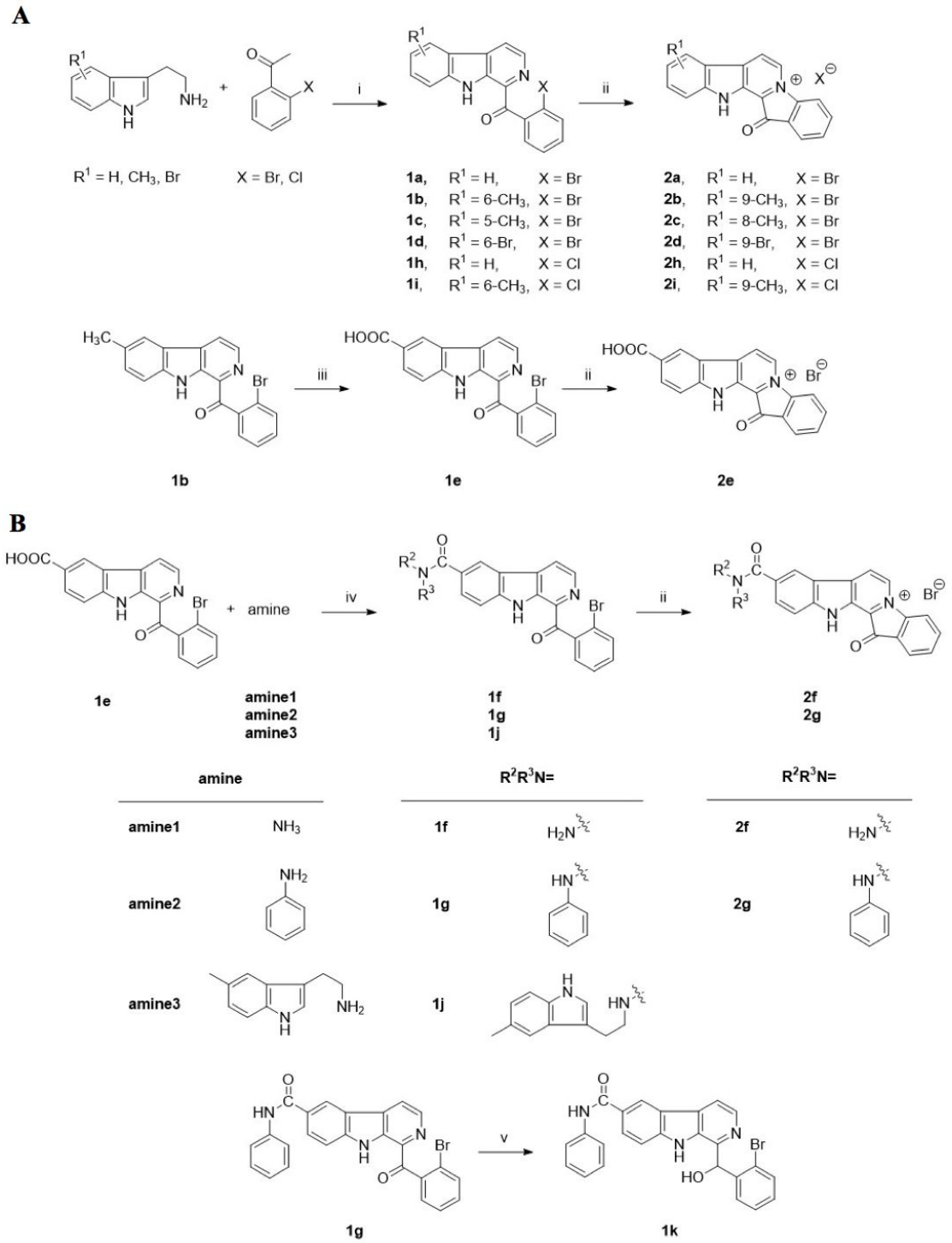
A
R1 = H, CH3, Br
X = Br, Cl
1a, R1 = H, X = Br
1b, R1 = 6-CH3, X = Br
1c, R1 = 5-CH3, X = Br
1d, R1 = 6-Br, X = Br
1h, R1 = H, X = Cl
1i, R1 = 6-CH3, X = Cl
2a, R1 = H, X = Br
2b, R1 = 9-CH3, X = Br
2c, R1 = 8-CH3, X = Br
2d, R1 = 9-Br, X = Br
2h, R1 = H, X = Cl
2i, R1 = 9-CH3, X = Cl
i
ii
iii
1b
1e
2e
B
amine
iv
1e
amine1
amine2
amine3
1f
1g
1j
2f
2g
R2R3N=
amine1
NH3
amine2
amine3
1g
v
1k

Figure 2

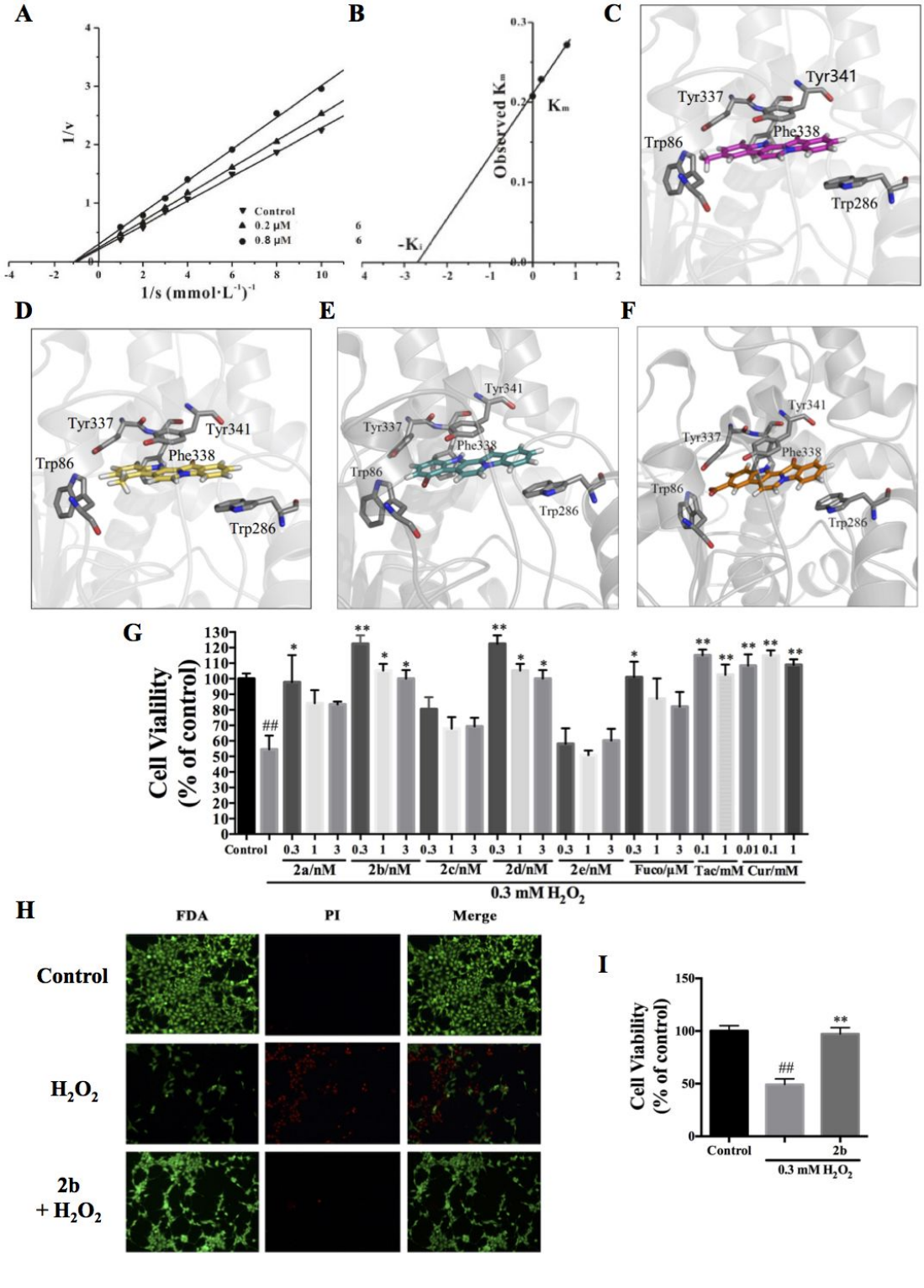
A
B
C
1/v
1/s (mmol·L⁻¹)⁻¹
Control
0.2 μM
0.8 μM
Observed Km
Km
-Ki
Tyr341
Tyr337
Phe338
Trp86
Trp286
D
E
F
G
Cell Viability (% of control)
Control
2a/nM
2b/nM
2c/nM
2d/nM
2e/nM
Fuco/μM
Tac/mM
Cur/mM
0.3 mM H2O2
H
FDA
PI
Merge
Control
H2O2
2b + H2O2
I
Cell Viability (% of control)
Control
2b
0.3 mM H2O2

Figure 3

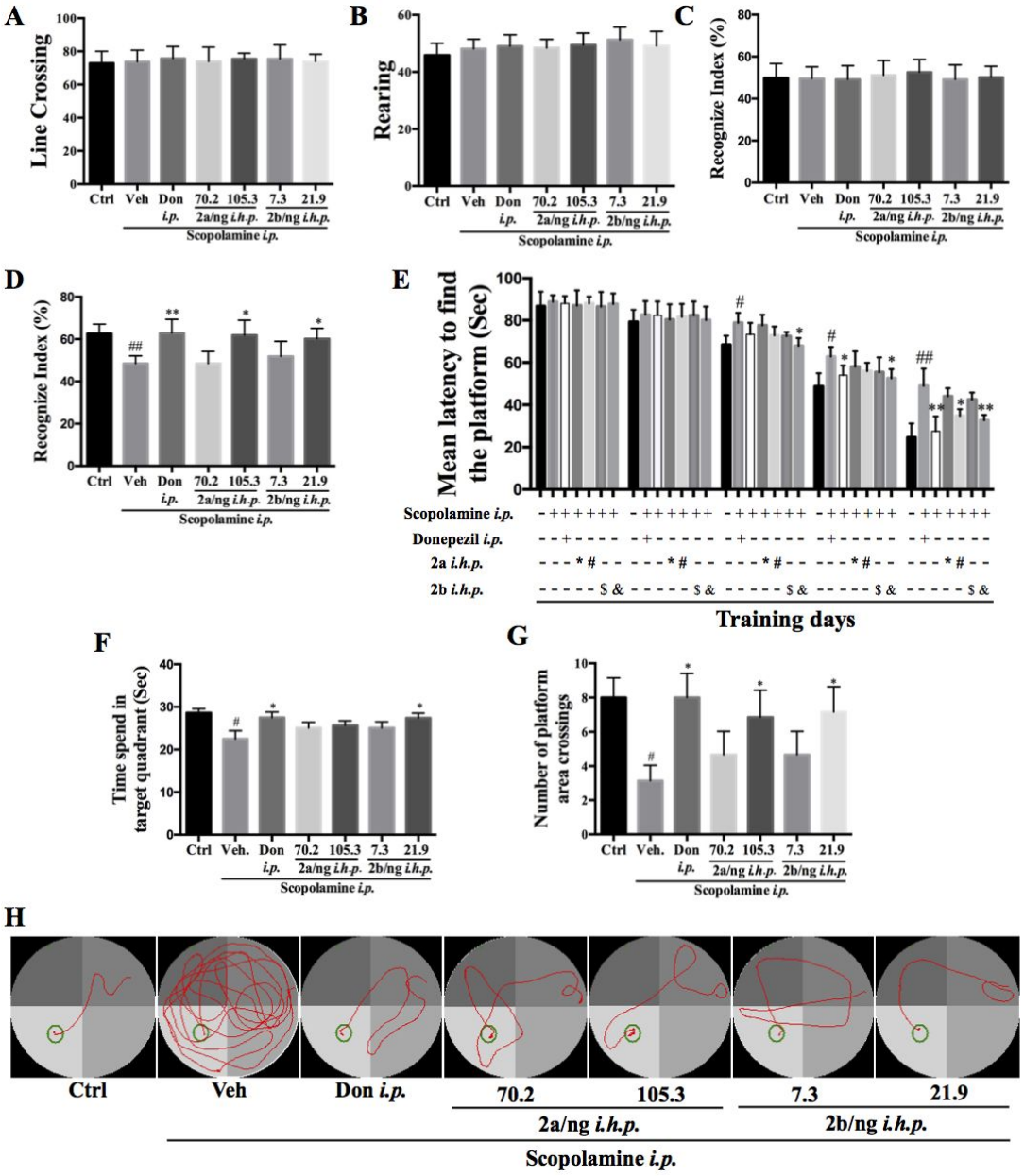
A
Line Crossing
B
Rearing
C
Recognize Index (%)
Ctrl Veh Don i.p. 70.2 105.3 2a/ng i.h.p. 7.3 21.9 2b/ng i.h.p.
Scopolamine i.p.
D
Recognize Index (%)
E
Mean latency to find the platform (Sec)
Scopolamine i.p.
Donepezil i.p.
2a i.h.p.
2b i.h.p.
Training days
F
Time spend in target quadrant (Sec)
G
Number of platform area crossings
H
Ctrl
Veh
Don i.p.
70.2
105.3
7.3
21.9
2a/ng i.h.p.
2b/ng i.h.p.
Scopolamine i.p.

Figure 4

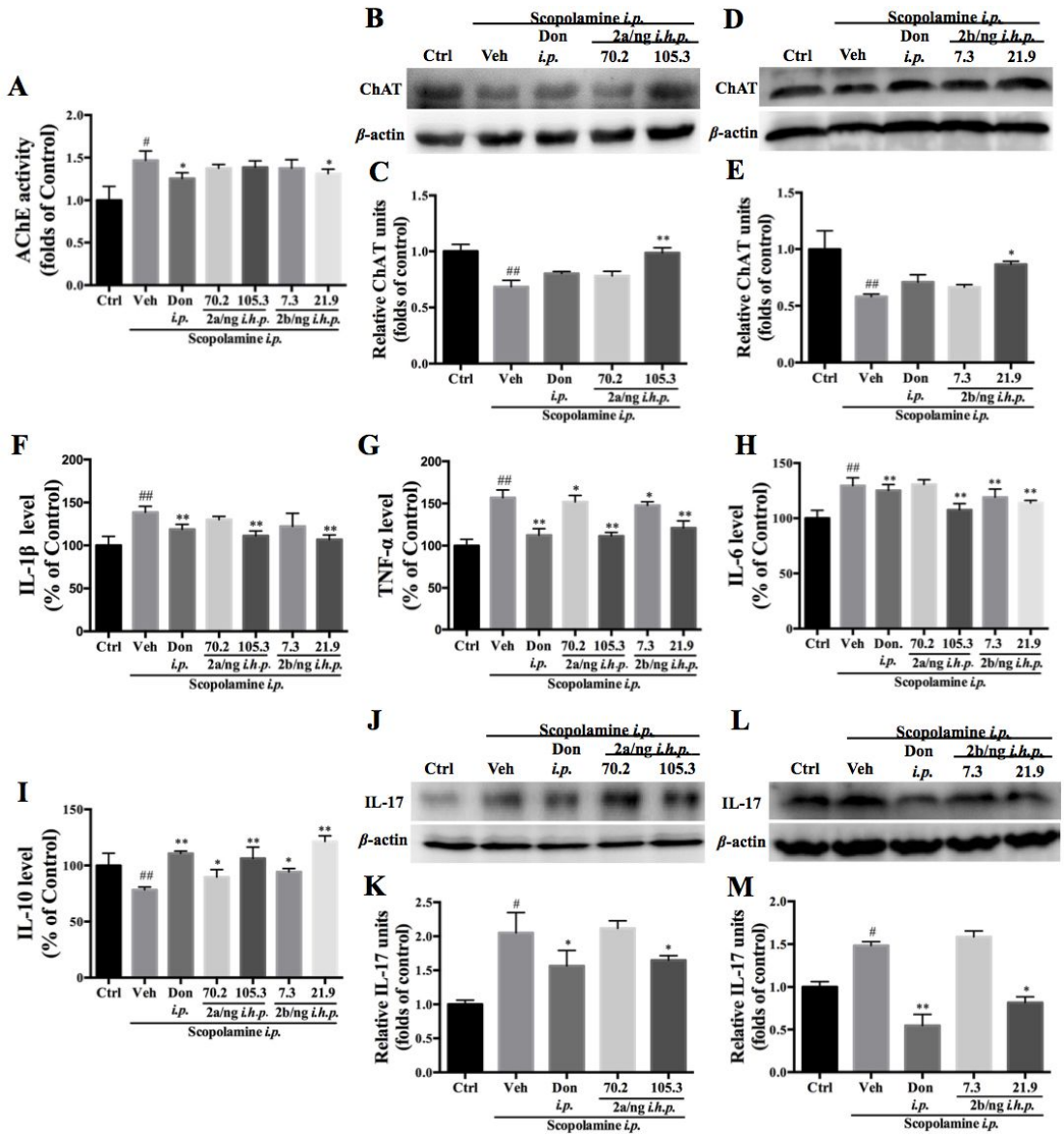
A
AChE activity (folds of Control)
B
ChAT
β-actin
Scopolamine i.p.
Ctrl
Veh
Don i.p.
2a/ng i.h.p.
70.2
105.3
C
Relative ChAT units (folds of control)
D
2b/ng i.h.p.
7.3
21.9
E
F
IL-1β level (% of Control)
G
TNF-α level (% of Control)
H
IL-6 level (% of Control)
I
IL-10 level (% of Control)
J
IL-17
K
Relative IL-17 units (folds of control)
L
M

Figure 5

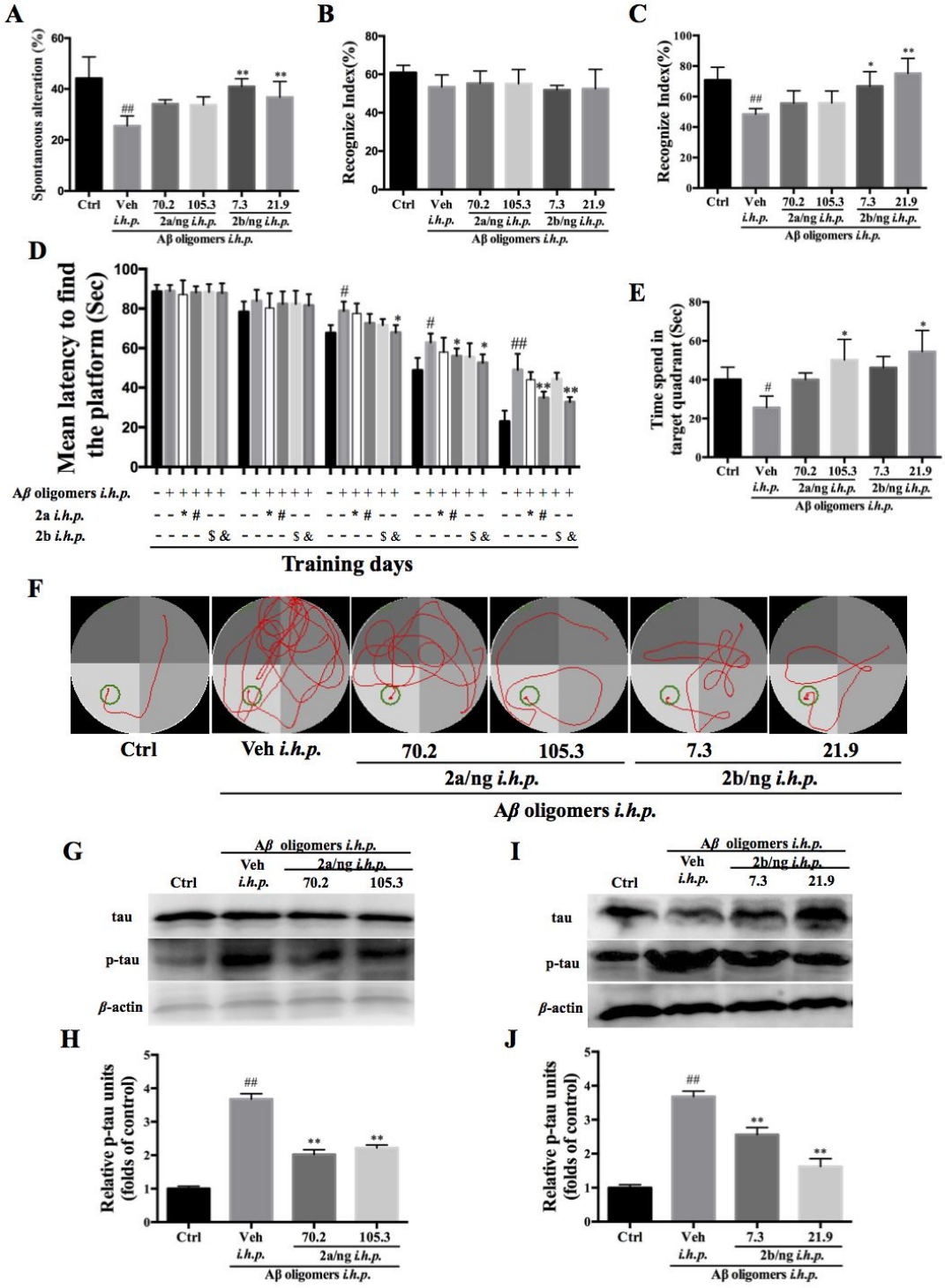
A
Spontaneous alteration (%)
B
Recognize Index(%)
C
Recognize Index(%)
Ctrl
Veh i.h.p.
70.2 105.3 2a/ng i.h.p.
7.3 21.9 2b/ng i.h.p.
Aβ oligomers i.h.p.
D
Mean latency to find the platform (Sec)
Aβ oligomers i.h.p.
2a i.h.p.
2b i.h.p.
Training days
E
Time spend in target quadrant (Sec)
F
Ctrl
Veh i.h.p.
70.2
105.3
7.3
21.9
2a/ng i.h.p.
2b/ng i.h.p.
Aβ oligomers i.h.p.
G
Aβ oligomers i.h.p.
tau
p-tau
β-actin
H
Relative p-tau units (folds of control)
I
J

Table 1. The inhibition activity of fascaplysin derivatives on AChE and BuChE.

Compound	IC_{50} (μM)[a]		SI[b]	Compound	IC_{50} (μM)[a]		SI[b]
	AChE	BuChE			AChE	BuChE	
1a	N.D.	N.D.	-[c]	**2a**	1.21 ± 0.04	8.63 ± 1.01	7.13
1b	N.D.	N.D.	-[c]	**2b**	0.95 ± 0.10	2.79 ± 0.76	2.94
1c	N.D.	N.D.	-[c]	**2c**	2.92 ± 0.09	11.11 ± 1.93	3.81
1d	N.D.	N.D.	-[c]	**2d**	2.32 ± 0.58	6.19 ± 0.87	2.67
1e	N.D.	N.D.	-[c]	**2e**	9.55 ± 1.23	15.98 ± 1.19	1.67
1f	N.D.	N.D.	-[c]	**2f**	N.D.	N.D.	-[c]
1g	N.D.	N.D.	-[c]	**2g**	N.D.	2.90 ± 0.21	-[c]
1h	N.D.	N.D.	-[c]	**2h**	1.28 ± 0.07	7.96 ± 0.67	6.22
1i	N.D.	N.D.	-[c]	**2i**	1.01 ± 0.22	2.92 ± 0.14	2.89
1j	N.D.	N.D.	-[c]	**Tacrine**	0.18 ± 0.01	0.23 ± 0.03	1.28
1k	N.D.	N.D.	-[c]	**Donepezil**	0.03 ± 0.01	2.13 ± 0.02	66.56

[a] The IC_{50} value was an average of three independent experiments.; [b] SI = IC_{50} (BuChE)/IC_{50} (AChE). [c] SI value could not be calculated. N.D. = cholinesterase inhibition was not detectable even when the concentration of chemicals above 1 mM. Data are expressed as the mean ± SD (n = 3).

Table 2. The IC_{50} values of compounds 2a, 2b, 2c, 2d, 2e to inhibit cell viability.

Compound	IC_{50} to inhibit cell viability (μM)
2a	0.09 ± 0.03
2b	0.18 ± 0.02
2c	1.60 ± 0.21
2d	5.30 ± 0.78
2e	75.80 ± 1.06

The IC_{50} value was an average of three independent experiments. Data are expressed as the mean ± SD (n = 3).

For Table of Contents Use Only

Fascaplysin Derivatives Are Potent Multi-target Agents Against Alzheimer's Disease: *in vitro* and *in vivo* Evidence

Hanbo Pan [1], Hongda Qiu [2], Ke Zhang [1], Panpan Zhang [1], Weida Liang [1], Mengxiang Yang [1], Chenye Mou [1], Miaoman Lin [2], Ming He [2], Xiao Xiao [1], Difan Zhang [1], Haixing Wang [3], Fufeng Liu [4], Yongmei Li [2], Haixiao Jin [5], Xiaojun Yan [5], Hongze Liang [2,*] and Wei Cui [1,4,*]

[1] Ningbo Key Laboratory of Behavior Neuroscience, Zhejiang Province Key Laboratory of Pathophysiology, School of Medicine, Ningbo University, Ningbo, 315211, China.

[2] School of Materials Science and Chemical Engineering, Ningbo University, Ningbo, 315211, China.

[3] Zhejiang Province Key Laboratory of Anesthesiology, Department of Anesthesiology, The Second Affiliated Hospital and Yuying Children's Hospital of Wenzhou Medical University, Wenzhou, 325000, China.

[4] State Key Laboratory of Food Nutrition and Safety, College of Biotechnology, Tianjin University of Science & Technology, Tianjin, 300457, China.

[5] Li Dak Sum Yip Yio Chin Kenneth Li Marine Biopharmaceutical Research Center, College of Food and Pharmaceutical Sciences, Ningbo University, Ningbo, 315800, China.

[*] Corresponding author: Prof. Hongze Liang, School of Materials Science and Chemical Engineering, Ningbo University, Zhejiang, China. Email: lianghongze@nbu.edu.cn.
and Dr. Wei Cui, Department of Physiology, School of Medicine, Ningbo University, Zhejiang, China. Email: cuiwei@nbu.edu.cn.